

**UV RAMAN INVESTIGATION OF PEPTIDE  
HYDRATION AND HYDROPHOBIC COLLAPSE**

by

Konstantin V Pimenov

B.S. Perm State University, 1996

Submitted to the Graduate Faculty of  
School of Arts and Sciences in partial fulfillment  
of the requirements for the degree of  
Master of Science

University of Pittsburgh

2007

UNIVERSITY OF PITTSBURGH  
SCHOOL OF ARTS AND SCIENCES

This thesis was presented

by

Konstantin Pimenov

It was defended on

April 20, 2007

and approved by

Sunil Saxena, Assistant Professor, Department of Chemistry

Christian Schafmeister, Assistant Professor, Department of Chemistry

Thesis Director: Sanford Asher, Distinguished Professor, Department of Chemistry

Copyright © by Konstantin Pimenov

2007

**UV RAMAN INVESTIGATION OF PEPTIDE  
HYDRATION AND HYDROPHOBIC COLLAPSE**

Konstantin Pimenov, M.S.

University of Pittsburgh, 2007

Hydration of an  $\alpha$ -helical, 21 residue, mainly Ala peptide was investigated by UV resonance Raman spectroscopy. UV resonance Raman spectra in the dehydrated solid state were compared to those in aqueous solution at different temperatures. The amide band frequencies of a dehydrated solid  $\alpha$ -helix peptide show frequency shifts compared to those in aqueous solution due to the loss of amide backbone hydrogen bonding to water; the amide II and amide III bands of the solid  $\alpha$ -helix downshift, while the amide I band upshifts. The shifts are identical in direction but smaller than those that occur for  $\alpha$ -helices in aqueous solution as the temperature increases; water hydrogen bonding strengths decrease as the temperature increases. The UV Raman amide band frequency shifts can be used to monitor  $\alpha$ -helix hydrogen bonding.

In addition, the phenomenon of hydrophobic collapse was investigated in poly(N-isopropylacrylamide) hydrogel nanoparticles.  $\sim 100$  nm hydrogel particles were synthesized and analyzed with variety of methods including UV resonance Raman (UVR) spectroscopy. The changes in UVR amide spectra are similar to those observed for peptide dehydration. The Raman bands associated with C-H stretching vibrations change in a manner expected to dehydration as well. Comparison of spectral changes of isopropyl group vibrations to that of amide group suggests different dehydration pattern of the two groups. Kinetics of the dehydration of the amide groups indicates a complex process, which can not be described by a two state model.

## TABLE OF CONTENTS

<b>PREFACE.....</b>	<b>X</b>
<b>1.0 INTRODUCTION.....</b>	<b>1</b>
<b>1.1 PROTEINS AND PROTEIN FOLDING PROBLEM.....</b>	<b>1</b>
<b>1.2 SECONDARY STRUCTURES.....</b>	<b>4</b>
<b>1.3 EXPERIMENTAL METHODS FOR STUDYING PROTEINS AND PEPTIDES.....</b>	<b>9</b>
<b>1.4 UV RESONANCE RAMAN SPECTROSCOPY.....</b>	<b>11</b>
<b>2.0 UV RAMAN EXAMINATION OF <math>\alpha</math>-HELICAL PEPTIDE WATER HYDROGEN BONDING.....</b>	<b>17</b>
<b>3.0 POLY(N-ISOPROPYLACRYLAMIDE) VOLUME PHASE TRANSITION.....</b>	<b>23</b>
<b>3.1 INTRODUCTION.....</b>	<b>23</b>
<b>3.2 EXPERIMENTAL.....</b>	<b>28</b>
<b>3.2.1 Sample preparation.....</b>	<b>28</b>
<b>3.2.2 Instrumentation.....</b>	<b>29</b>
<b>3.3 RESULTS AND DISCUSSION.....</b>	<b>31</b>
<b>3.3.1 UV Raman Spectra. Amide Region.....</b>	<b>32</b>
<b>3.3.1.1 AmIII.....</b>	<b>36</b>
<b>3.3.1.2 C-H<sub>b</sub>.....</b>	<b>38</b>

3.3.1.3	AmII.....	39
3.3.1.4	AmI.....	40
3.3.2	Visible Raman. C-H stretching region.....	46
3.3.3	Kinetics of the phase transition .....	54
3.4	CONCLUSIONS.....	62
4.0	DEVELOPMENT OF NEW MARKERS OF PEPTIDE CONFORMATIONS. C <sub>A</sub> -H STRETCHING.....	64
	BIBLIOGRAPHY.....	67

## LIST OF FIGURES

Figure 1. Generic Structure of an Amino Acid.....	1
Figure 2. Funnel-like energy landscape describing protein folding. A: 2 state model; B: many intermediate states are included. (adapted from Ken Dill's web site: <a href="http://www.dillgroup.ucsf.edu">http://www.dillgroup.ucsf.edu</a> ).....	4
Figure 3. Representation of peptides in $\alpha$ -helical conformation. A) Schematic representation of a 5-mer. B) 3-D view of (Ala) <sub>14</sub> .	5
Figure 4. $\Phi$ and $\Psi$ angles of trialanine.....	5
Figure 5. Types of $\beta$ -sheets: parallel and anti-parallel. Stabilizing hydrogen bonds are shown in green for parallel $\beta$ -sheet and in red for anti-parallel $\beta$ -sheet.....	6
Figure 6. The Ramachandran plot of a polypeptide. Lowest energy allowed regions are shown in red, while less stable areas are yellow. ....	7
Figure 7. Schematic diagram, comparing IR absorption, and different forms of Raman scattering. ....	12
Figure 8. Atomic motion of amide bands. ....	14
Figure 9. Sample spectrum of poly-L-lysine .....	15

Figure 10. 204 nm UV resonance Raman spectra of A: solid sample obtained by freezing a -5 °C AP solution and lyophilizing (~63 %  $\alpha$ -helix). B: solid sample obtained by evaporating 40 °C AP solution. C: calculated spectrum of pure  $\beta$ -sheet PGA-PLL stoichiometric mixture in solution at 70 °C. A-B: solid AP  $\alpha$ -helix spectrum calculated by subtracting spectrum B from spectrum A. Lower spectra are pure  $\alpha$ -helix AP solution spectra at the indicated temperatures..... 20

Figure 11. Transparent NIPAM solution at 25 °C. Swollen particles, ~ 200 nm diameter. .... 24

Figure 12. Turbid NIPAM solution at 45 °C. Collapsed particles, ~ 50 nm diameter. .... 25

Figure 13. Schematic representation of the transition. .... 25

Figure 14. TEM image of PNIPAM particles..... 30

Figure 15. Turbidity of NIPAM solution measures ad 500 nm. .... 32

Figure 16. 204 nm excited UV Raman spectra of NIPAM and NIPAM-d<sub>7</sub> at temperatures below and above the transition, as well as the spectra of AP and PLL..... 34

Figure 17. Repeat unit of poly(N-isopropylacrylamide chain)..... 35

Figure 18. Temperature dependence of PNIPAM aqueous solution amide spectra ..... 37

Figure 19. Temperature dependence of NIPAM-d<sub>7</sub> sample in water..... 38

Figure 20. Modeling of the AmI and AmII spectral region for 15 °C spectrum of NIPAM..... 41

Figure 21. Modeling of the AmI and AmII spectral region for 35 °C spectrum of NIPAM..... 42

Figure 22. Modeling of the AmI and AmII spectral region for 55 °C spectrum of NIPAM..... 42

Figure 23. Intensity ratio of the AmI band components comparing to turbidity. .... 43

Figure 24. Particle size comparing to AmI and AmIII frequency. .... 45

Figure 25. C-H stretching vibrations of iPrOH in its aqueous solutions. 488 nm excitation ..... 49

Figure 26. 488 nm excited Raman spectra of PNIPAM and PNIPAM-d<sub>7</sub> in comparison to isopropanol..... 50

Figure 27. 204 nm excited spectra of isopropanol and PNIPAM D <sub>2</sub> O solution. ....	51
Figure 28. 488 nm excited Raman spectra of PNIPAM at indicated temperatures. ....	52
Figure 29. Comparison of different spectroscopic markers of PNIPAM transition: Position of C-H stretching peak; Turbidity of the solution; Ratio of Amide I peaks.....	53
Figure 30. 204 nm transient spectra of NIPAM at selected delay times.....	54
Figure 31. An example of transient spectra modeling. ....	55
Figure 32. Difference spectra hot-cold at indicated delay times. ....	57
Figure 33. Difference spectra obtained by subtraction of steady state spectra at indicated temperatures.....	58
Figure 34. Time dependence of AmI and AmIII intensities in difference spectra. ....	60
Figure 35. 488 nm excited Raman spectra of Ac-Ala-NH <sub>2</sub> in the solid state and solution at a concentration of 10 mg/ml. ....	66

## PREFACE

I would like to express my gratitude to my research advisor Prof. Sanford A. Asher, who guided me through the course of my study and stimulated my thoughts. I also thank my thesis committee members Prof. Sunil Saxena and Prof. Christian Schafmeister for their helpful suggestions during the manuscript preparation as well as discussions that helped me to finish my projects. Special thanks to my senior coworkers Dr. Vladimir Alexeev, Dr. Matti Ben-Moshe, Dr. John Jackovitz, Dr. Adrian Murza, Dr. Nataliya Myshakina, Dr. Alex Goponenko, and Dr. Jon Scaffidi for their help in introducing me to the theoretical and experimental aspects of spectroscopy and colloid science. I also thank my graduate student peers: Sergei Bykov, Zeeshan Ahmed, Bhavya Sharma, Justin Baca, Michelle Muscatello, Sylvere Sirikare, Benjamin Kabagambe, Jeremy Walker, Kyle Kimble, Justin Bohn, Jia Luo, and Lu Ma for their participation in my research projects and creating productive environment in the group. I should especially acknowledge Alexander Mikhonin who contributed to my professional growth on a daily basis.

And last, but not least I am in debt to my family: my wife Natalia and daughter Veronica who have been with me at all times helping out through all the struggles of graduate work and helping to remember that the family is the utmost goal of any professional career.

## 1.0 INTRODUCTION

### 1.1 PROTEINS AND PROTEIN FOLDING PROBLEM

Proteins are essential constituents of living organisms. Almost every aspect of cellular life involves proteins. They are involved in the expression of genetic information, transport of cellular elements, and catalysis of chemical reactions. Proteins are necessary components of muscles and bones. They participate in processes of cell recognition and signaling, energy conversion and storage as well as many other functions.<sup>1</sup> The huge variety of protein functions relates to their diverse properties and structures.

Proteins are biological polymers build up of amino acids linked by peptide bonds. Each protein is characterized by its unique length, sequence and most importantly, three dimensional structure. There are 20 types of naturally occurring amino acids that can be incorporated into a protein. All amino acids (except proline) have the general structure shown in Figure 1. Each amino acid has its unique sidechain R. The functional diversity of proteins mentioned above comes from the variety of three-dimensional structures that proteins can form utilizing different sequences of these 20 amino acids.

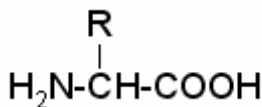


**Figure 1.** Generic Structure of an Amino Acid.

Several levels of protein structure are recognized.

The number and the sequence of amino acids comprising a protein is referred to as its *primary structure*.

Next, a polypeptide chain adopts specific conformation stabilized by non-covalent interactions – hydrogen bonding between amides of different peptide bonds. This is a protein's *secondary structure*.  $\alpha$ -helix and  $\beta$ -sheet are among the most important types of secondary structures.

When  $\alpha$ -helices or other secondary structure elements are organized into a larger structure by means of sidechain interactions (both non-covalent and disulfide bridges) a *tertiary structure* is formed.

Organization of two or more polypeptide chains (domains) into a single functional protein is referred to as *quaternary structure*.

As soon as proteins get into favorable environment they adopt specific three-dimensional conformation with all levels of structure. Such a conformation is referred to as native state and allows for biological activity. A transformation from non-ordered conformation to biologically active native state is described as protein folding. It is obvious that folding process is of great importance, and thus researches have been actively studying the phenomenon for the last several decades. In spite of years of effort the protein folding is still appears as mysterious and largely unexplained phenomenon. About 50 years ago it was proposed that protein primary structure (amino acid sequence) entirely encodes the protein folding pathway<sup>2</sup> (for proteins that fold without chaperones). However, the rules that govern this process are still unclear. It is still impossible to predict three-dimensional protein structures from primary sequences unless these sequences have been previously observed in a protein of known structure. That makes the

mechanism of protein folding a major unsolved challenge in the understanding of biological structure and function. The lack of understanding of protein folding rules is usually referred to as “protein folding problem”.

Solving the protein folding problem will greatly advance biological sciences. Understanding the protein folding mechanisms will permit the detailed insight into the origin of many diseases. It will enable the design of drugs to alleviate disease, possibly to intervene and refold proteins. An understanding of protein folding will dramatically impact the field of genetic engineering, which will aid the development of new products for agriculture and medicine.

To illustrate the protein folding problem one may consider the Levinthal paradox. It refers to an apparent problem when the protein folding process is described as a random search of the most stable conformation. For example, small size protein of 100 amino acids would have at least  $2^{100}$  (or  $10^{30}$ ) different conformations, providing that each residue may exist in 2 states. The random search of the lowest energy conformation (the native state) would require about  $10^{11}$  years, if we assume transition from one conformation to another takes  $10^{-12}$  sec which is based on the average rotational frequency around a chemical bond. An experimental fact, however, is that most proteins fold in much less than a second. This apparent paradox originally described by Levinthal<sup>3</sup> clearly indicates, that the folding process does not occur through a random search of conformations, rather it proceeds through a certain pathway, at least part of which has to be “known” by protein from its primary structure.

A great number of models have been proposed for the folding process in general, or for the specific folding of a particular protein. Most of them avoid the Levinthal paradox by postulating that proteins dramatically narrow their conformational freedom during first very fast step which is governed by a hydrophobic collapse. The non-native conformations are very close

in energy so transition between these states is fast. The native state is much lower in energy. This energy landscape diagram corresponding to such model is show in Figure 2.

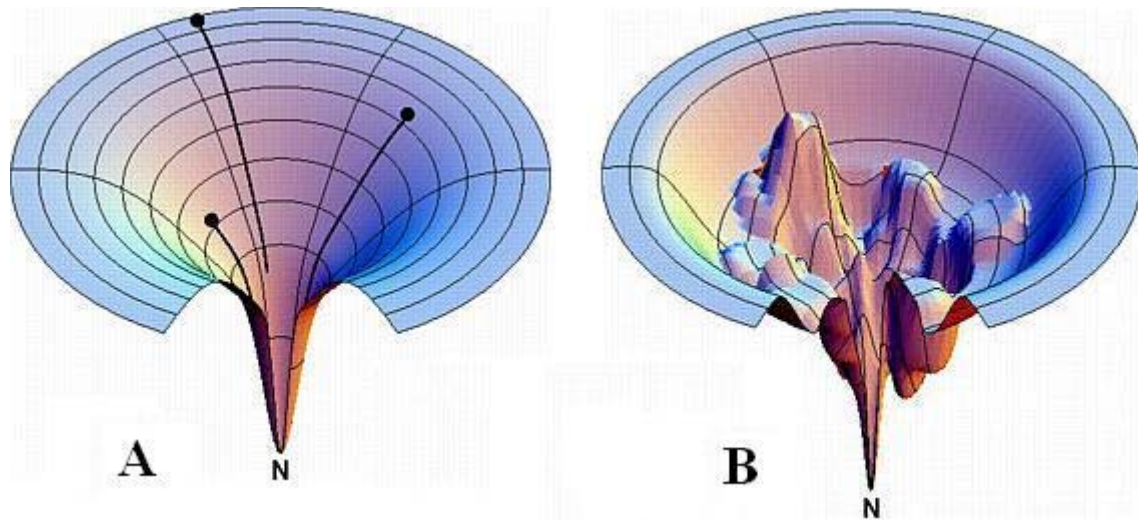


**Figure 2.** Funnel-like energy landscape describing protein folding. A: 2 state model; B: many intermediate states are included. (adapted from Ken Dill’s web site: <http://www.dillgroup.ucsf.edu>).

## 1.2 SECONDARY STRUCTURES

In order to better understand the process of folding, protein’s folded states need to be characterized in greater detail.  $\alpha$ -helix and  $\beta$ -sheet are the most common protein secondary structure motifs. Figure 3 shows both schematic diagram and 3-D view of a polypeptide chain in  $\alpha$ -helical conformation. Hydrogen bonding between amide nitrogen of the residue  $i$  and carbonyl oxygen of residue  $i+4$  stabilizes the conformation. In order to form hydrogen bond the participating residues need to be oriented in a certain way in space. Each residue is characterized

by a pair of dihedral angles that define its orientation. Figure 4 shows  $\Phi$  and  $\Psi$  angles in alanine tripeptide. Since C-N bond carries a partial double character, atoms O, C, N, H in a peptide bond lay in planes (green rectangles) which can rotate around  $C_{\alpha}$ -C and N- $C_{\alpha}$  bonds. Values of  $\Phi$  and  $\Psi$  angles describe positions of these planes.

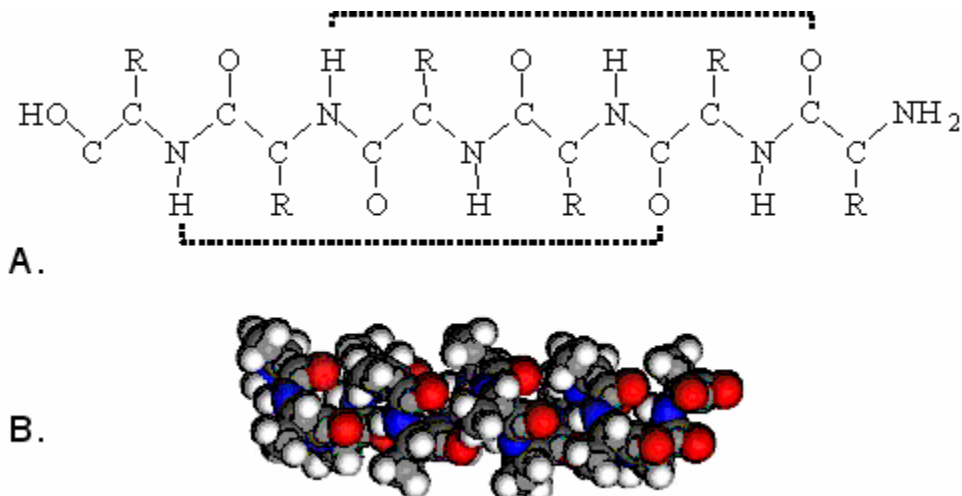


**Figure 3.** Representation of peptides in  $\alpha$ -helical conformation. A) Schematic representation of a 5-mer. B) 3-D view of (Ala)<sub>14</sub>.

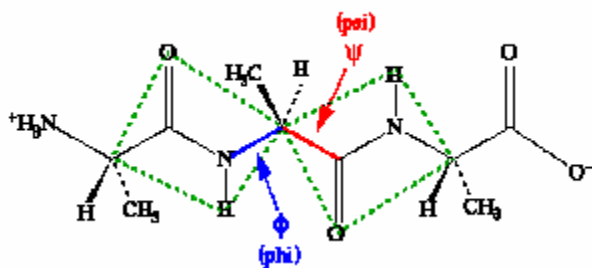


**Figure 4.**  $\Phi$  and  $\Psi$  angles of trialanine.

In  $\alpha$ -helical conformation the angles are  $\Phi = -57^\circ$  and  $\Psi = -47^\circ$ .

$\beta$ -sheet is second most abundant secondary structure. It has the angles  $\Phi = -139^\circ$  and  $\Psi = -135^\circ$ . It consists of several strands of extended polypeptide chains which stick to one another via hydrogen bonding. Each individual strand does not have intrachain hydrogen bonds, so it is not stable by itself. Strands are stable when incorporated into sheets where strands are held together via interstrand hydrogen bonding. There are 2 types of  $\beta$ -sheet structures depending on the mutual orientation of strands. In parallel  $\beta$ -sheet the neighboring strands propagate into the same direction (i.e. direction from N terminus to C terminus are the same), while in anti-parallel  $\beta$ -sheet adjacent chains are aligned in opposite directions. Figure 5 shows arrangement of peptide chains in  $\beta$ -sheet structure.

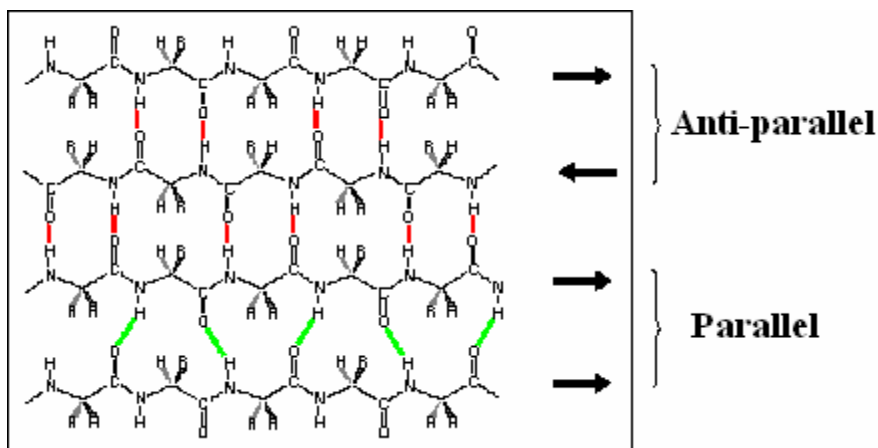


**Figure 5.** Types of  $\beta$ -sheets: parallel and anti-parallel. Stabilizing hydrogen bonds are shown in green for parallel  $\beta$ -sheet and in red for anti-parallel  $\beta$ -sheet.

The values of  $\Phi$  and  $\Psi$  angles are not always identical for the same type of secondary structure in different proteins. Variations are not large, however, since rotations are hindered by neighboring residues and sidechains. Ramachandran was first who discussed these steric constraints and proposed a map that shows allowed regions of  $\Phi$  and  $\Psi$  angles for different

secondary structure motifs.<sup>4,5</sup> Such representation got the name Ramachandran plot. Figure 6 shows a typical Ramachandran plot of a polypeptide. The plot applies for any residue except Proline and Glycine since the former has greatly restricted conformational space, while latter provides almost no restrictions at all.

The ultimate configuration that a polypeptide chain adopts depends on various factors. As mentioned above, polypeptide chain with its sidechains puts steric constraints on rotation around  $\Phi$  and  $\Psi$  angles. Next, different interactions are pushing the chain around within allowed Ramachandran space. Such interaction include: electrostatic, hydrogen bonding, Van der Waals, and hydrophobic forces. All of these include interactions between peptide itself as well as interactions with surroundings.

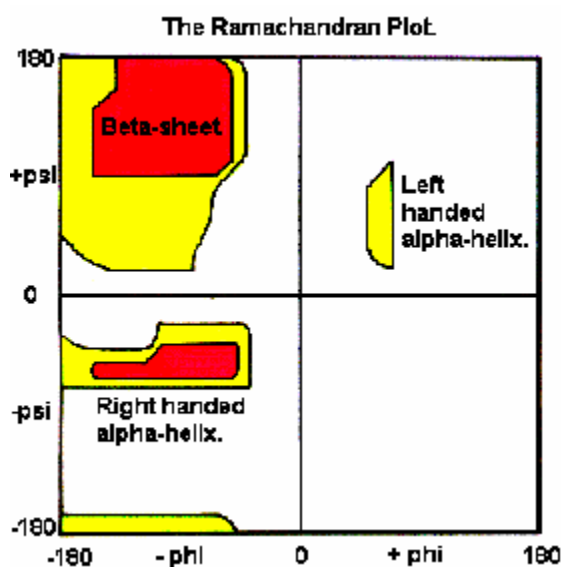


**Figure 6.** The Ramachandran plot of a polypeptide. Lowest energy allowed regions are shown in red, while less stable areas are yellow.

*Electrostatic interactions* between ionizable sidechains such as the carboxylate of Aspartic and Glutamic acid and amine of Lysine and Glutamine add further stability to the native

state. Ionizable groups are also surrounded by layers of particularly oriented water molecules, as well as by any ionic solutes present in the environment. It has been shown, that electrostatic interactions play a significant role in protein folding.<sup>6-8</sup>

Although the most of the peptide *hydrogen bonding* potential is used to stabilize conformation, (intrachain hydrogen bonds in  $\alpha$ -helix, interchain hydrogen bonding in  $\beta$ -sheet) There is still a possibility for additional hydrogen bonding. The carbonyl oxygen is capable of 2 hydrogen bonds since it has 2 lone pairs of electrons available. Only one of them is engaged in peptide-peptide hydrogen bonding, leaving the other a possibility to hydrogen bond to a solvent molecule. There are also situations, where water molecule interacts with peptide-peptide hydrogen bond forming a three centered hydrogen bond.<sup>9,10</sup> In some secondary structures (polyproline II conformation for example) peptide-water interactions are the only existing hydrogen bonding stabilizing the conformation.

*Van der Waals* interactions or dispersion force is the weakest of all interactions involved in protein folding. This weak attraction occurs between any atoms, but it is important only if stronger interactions are absent. Van der Waals forces are usually considered for methyl group and longer hydrocarbon chains. Although single methyl-methyl interaction is insignificantly weak, a large number of such interactions in the hydrophobic core of protein can be quite significant.<sup>7,8,11</sup>

*Hydrophobic interactions* constitute the most obscure class of interactions in biophysics<sup>8</sup>. Much confusion exists in the literature as to the exact contribution and nature of hydrophobic interactions in protein folding. In the simplest example, the hydrophobic force is referred to a preference of non-polar solutes to each other comparing to being surrounded by water. The concept of hydrophobicity was used to explain the low solubility of non-polar solutes in water

and the subsequent changes in physical properties of water observed upon dissolution of non-polar solutes.<sup>12</sup> According to this rationalization, introduction of non-polar solutes into water leads to formation of clathrates or cage like structures in water that surrounds the non-polar solutes. Such ordered structure is a low entropy state, resulting in an overall reduction in the entropy of the system. Thus, free energy of solvation is reduced. Although there is a lot of vagueness in hydrophobic arguments it is now well accepted, that hydrophobic interactions play a major role in protein folding, especially on early stages, where hydrophobic collapse takes place narrowing the number of conformations and preventing the Levinthal paradox.

### **1.3 EXPERIMENTAL METHODS FOR STUDYING PROTEINS AND PEPTIDES**

A number of *experimental techniques* are being used to study protein and peptide structure and dynamics. These include X-ray crystallography,<sup>13</sup> NMR,<sup>14,15</sup> EPR,<sup>16</sup> Infrared (IR) and Fluorescence spectroscopy,<sup>17-23</sup> Circular Dichroism (CD),<sup>24-26</sup> Raman Optical Activity (ROA),<sup>10,27-29</sup> Raman,<sup>30,31</sup> and UV Resonance Raman Spectroscopy (UVR).<sup>26,32-37</sup>

X-ray crystallography provides the most detailed information about the three dimensional structure of protein. Resolutions of fractions of an Å can be achieved. However, typical X-ray experiment requires a crystalline sample, in which a protein most likely exists in a form different from its biologically active native state. Thus, the relevance of data is always a concern. It also eliminates the possibility of studying dynamic events. Although highly sophisticated kinetic x-ray methodologies are being developed, they only allow to study events on a timescale of tens of milliseconds with resolution not better than hundreds of microseconds.

NMR on the other hand, is able to study solutions, thus it is possible to get insight into conformations that are similar to a native state. Much like X-ray, NMR can provide detailed information on the local and global structure of the protein. The method has its limitations, however. Large proteins are difficult to study due to spectral congestion and line broadening. Even sophisticated techniques like four dimensional NMR spectroscopy allows studying proteins only up to 150 residues long.<sup>14,15</sup> Another inherent problem is the requirement for high peptide/protein concentrations which sometimes results in aggregation and precipitation. Further, the time scale of typical NMR experiments limits kinetic resolutions to the millisecond time regime, which misses important early stage events.<sup>8,38</sup>

Absorption techniques use signals from either amide chromophore in IR, or from some artificial labeling groups in visible region. IR absorption measurements directly probe the polypeptide backbone secondary structure, however, only the Amide I region is available for quantitative studies.<sup>39</sup>

Fluorescence can be used to probe solvent exposure of aromatic chromophores, motional anisotropy and the formation of specific tertiary contacts. Intrinsic fluorescence of proteins without artificial labels derives from the aromatic residues, mainly tryptophan. Quenchers such as acrylamide can be used to probe solvent accessibility. Although the fluorescence spectrum, lifetime and quantum yield do not simply report on protein structure, fluorescence measurements have yielded useful information on formation of protein tertiary contacts during the folding.<sup>40,41</sup>

CD spectra probe the secondary structure of the polypeptide backbone, especially Far-UV CD, since the  $n \rightarrow \pi^*$ ,  $\pi \rightarrow \pi^*$  electronic transitions of the amide group contribute to CD signal at 180-230 nm. Far-UV CD is widely used to quantitatively analyze protein secondary structure.<sup>42,43</sup> Near-UV CD can describe some tertiary structure changes during protein folding.

However, while CD can provide information about the secondary structure of the protein with relative ease, it suffers interference from the  $\pi \rightarrow \pi^*$  transition of the aromatic residues. Due to this interference estimation of secondary structure content ( $\alpha$ -helix in particular) is at times a difficult task.<sup>44,45</sup>

Given the shortcomings of the techniques discussed above, UVRRS offers the best compromise in terms of information content, kinetic resolution, and relative ease of handling.

#### **1.4 UV RESONANCE RAMAN SPECTROSCOPY**

Raman spectroscopy is one of the fundamental types of spectroscopy used to infer the molecular structure and properties from vibrational transitions.<sup>46</sup> In many aspects it is similar to IR spectroscopy, but has its individual features. In contrast to IR, where radiation is absorbed by a sample, Raman experiment deals with radiation inelastically scattered by a molecule of interest. Thus, Raman scattering is a two photon event. The light scattered by a molecule consists of two types of scattered light: Rayleigh and Raman. Raman scattered light, in turn consists of Stokes, and Anti-Stokes emission. Schematic representation of the Raman effect is shown in Figure 7.

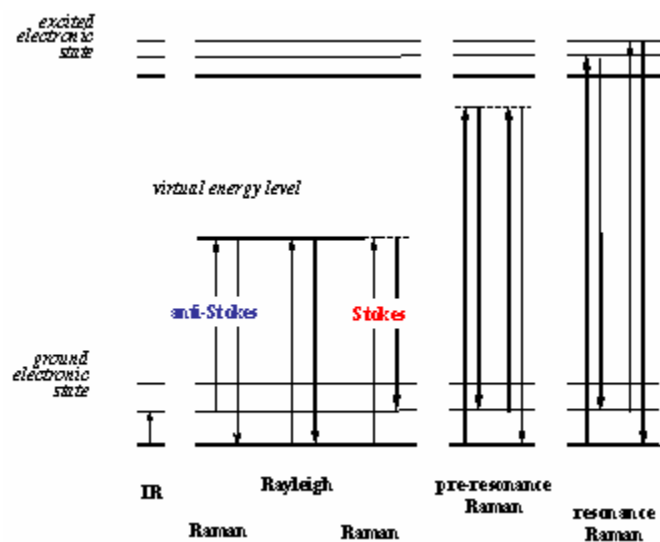


**Figure 7.** Schematic diagram, comparing IR absorption, and different forms of Raman scattering.

Incident radiation excites a molecule from its ground electronic state to some intermediate *virtual* state, which scatters light and returns the molecule to the same or different vibrational state. Most of light undergoes Rayleigh scattering, where initial and final vibrational states are the same. Thus, scattered light has the same frequency as the incident light, so Rayleigh scattering constitutes an elastic type of scattering. Small part of light however, interacts with a molecule in such a way, that scattered light has frequency less than that of incident light. In this case the molecule ends up in a higher energy vibrational state. This phenomenon is called Stokes scattering. Since energy difference between incident and scattered light corresponds to a difference in vibrational energy levels, scattered light carries information about properties of the molecule. The ratio of molecules that produce Stokes scattering to those that do Rayleigh depends on the Boltzmann factor. This is manifested in relative intensities of Rayleigh and Stokes lines. Even smaller fraction of molecules interacts with light in such a way that molecules get transferred to a lower vibrational level of the ground electronic state. In this case scattered light is of higher frequency than incident light was. This is anti-Stokes scattering phenomenon.

The number of molecules that undergo such transition, and consequently intensity of the detected signal is several orders of magnitude smaller than that of Stokes scattering. This is because molecules that produce anti-Stokes scattering have to initially be in the states higher than ground vibrational state, which is at room temperature constitutes a very small fraction of the sample.

Normal or non-resonant Raman scattering involves excitation by light of energy much less than the difference between ground and excited electronic states. Resonance Raman scattering occurs when energy of exciting radiation is comparable to the difference between ground and excited electronic states. Same three types of processes occur for resonance Raman: Rayleigh, Stokes, and anti-Stokes scattering. Intensity of some bands in resonance Raman spectrum are orders of magnitude higher than that of normal Raman bands. There are particular excitation frequencies that allow for such resonance. They are molecular electronic absorption frequencies. The resonance enhancement factor can be as high as  $10^8$ .<sup>32,33</sup>

The resonance Raman effect leads to selectivity of Raman measurements. The same analyte produces different Raman spectra depending on excitation wavelength, especially if different segments of the molecule have different absorption bands. For example, excitation within ~230 nm is in resonance with aromatic amino acids tyrosine, tryptophan and phenylalanine. Numerous UV Raman studies used this selective enhancement to monitor hydrogen bonding and solvent exposure of these residues in proteins.<sup>34,47,48</sup>

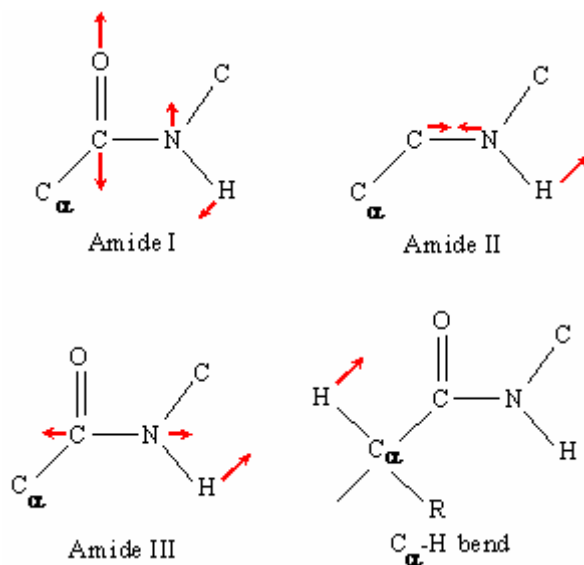


**Figure 8.** Atomic motion of amide bands.

The peptide bond itself has an absorption band around 190 nm, so excitation of proteins and peptides with  $\sim 200$  nm selectively enhances peptide backbone amide vibrations.<sup>49</sup> The resultant spectra are dominated by amide vibrations, designated as Amide I, II, III, and  $C_{\alpha}$ -H bending. Figure 8 shows atomic motions associated with these vibrations, and Figure 9 demonstrates example of these bands in a spectrum of a polypeptide poly-L-lysine.

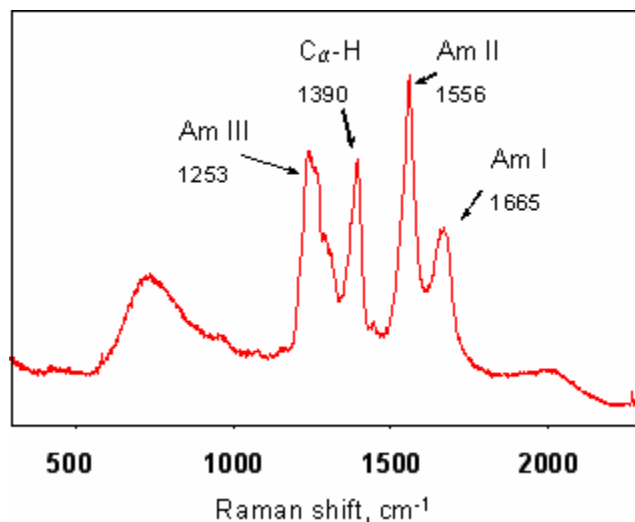


**Figure 9.** Sample spectrum of poly-L-lysine

As mentioned previously, the spectrum is relatively simple since only amide backbone vibrations are resonantly enhanced. Further, the spectrum carries easily recognizable features of different secondary structure elements. Using a library of proteins of known structure, Chi *et al*<sup>49</sup> developed a methodology to correlate the UV Raman spectral markers with presence of secondary structure motifs. This methodology allowed to quantitatively determine the amount of  $\alpha$ -helix,  $\beta$ -sheet and random coil content of large proteins. Recent work by Asher *et al*<sup>35</sup> has suggested that the alanine based, mostly helical peptide AP melts from  $\alpha$ -helical structure to a polyproline II (PPII) type helix conformation. These results offer further support to recent theoretical studies that have suggested that the small peptides in their unordered state, adopt a predominantly PPII helix conformation.<sup>36,50-55</sup> As mentioned above UV Raman spectroscopy is able to study very fast kinetics. Lednev *et al*<sup>36</sup> performed kinetic measurements of AP peptide with a temporal resolution of 3 nsec. Such resolutions allow experimentalists to capture the earliest steps in protein folding which are not accessible by other experimental techniques.

As it can be seen from the above discussion UV Resonance Raman spectroscopy is uniquely suitable to advance the field of protein folding and holds the promise to further our understanding of the fundamental principles such complicated phenomenon.

## 2.0 UV RAMAN EXAMINATION OF $\alpha$ -HELICAL PEPTIDE WATER HYDROGEN BONDING

Both intramolecular protein-protein interactions and protein-solvent interactions determine native protein secondary and tertiary structures. For example, intramolecular protein hydrogen bonding stabilizes  $\alpha$ -helical and  $\beta$ -sheet conformations,<sup>1,9,10</sup> while protein-water interactions stabilize peptide and protein PPII conformations.<sup>50,51,56,57</sup> However, even though intramolecular hydrogen bonding is expected to dominate the amide carbonyl and N-H hydrogen bonding of  $\alpha$ -helical peptides, an exterior sheath of water should hydrogen bond to exposed intramolecularly bonded N-H--O=C linkages.<sup>9,58-60</sup> Such interactions may also be important in the stabilization of the  $\alpha$ -helix conformation.<sup>19,61,62</sup> These hydrogen bonding interactions are expected to depend upon the extent that the peptide sidechain shields the peptide backbone from water.

In this work we directly examine water hydrogen bonding to the backbone of  $\alpha$ -helix peptides by comparing UV Raman spectra of an  $\alpha$ -helical peptide between aqueous solution and the dehydrated solid state. We are examining the extent of hydrogen bonding to  $\alpha$ -helices and the consequence of this hydrogen bonding to the amide vibrational spectra. One of our goals is to develop a method to monitor this hydrogen bonding.

We previously demonstrated that the UV Raman amide band spectra are sensitive to both the peptide secondary structure composition<sup>36,49,63</sup> and peptide-water interactions.<sup>35,36</sup> By

exciting the spectra within the  $\sim 200$  nm peptide bond  $\pi \rightarrow \pi^*$  transitions we can excite UV Raman spectra dominated by the peptide bond vibrations.<sup>49</sup>

We examine here the hydrogen bonding interactions of a 21 residue, mainly ala peptide (AP) that at low temperature exists in an equilibrium between  $\alpha$ -helical and PPII conformations.<sup>35,36,64</sup> We previously characterized the temperature dependence of the  $-5 - 30$  °C AP  $\alpha$ -helical Raman spectra<sup>64</sup> by subtracting appropriate amounts of the PPII conformation Raman spectra from the experimentally measured spectra at each temperature. We observed that the amide bands of both the  $\alpha$ -helix and PPII conformations undergo characteristic changes with temperature which we earlier postulated derived from weakening of water hydrogen bonding as the temperature increases.

In the work here we prepared an  $\alpha$  helical solid AP sample by quickly freezing a solution of AP initially at  $-5$  °C (where the  $\alpha$ -helix content<sup>36</sup> is  $\sim 63$  %) in liquid nitrogen. The frozen sample was then dehydrated by lyophilization at low temperature, after which it was warmed to room temperature under vacuum. We expect that this process results in a solid AP sample which contains significant amounts of  $\alpha$ -helix as well as other conformations, which probably include  $\beta$ -sheet,  $\beta$ -strand, and disordered conformations, with some non-hydrogen bonded amide bonds. It is known that polyalanine can occur in  $\alpha$ -helix<sup>65</sup> or  $\beta$ -sheet<sup>1</sup> conformation in the solid phase. We also prepared a solid AP sample which we expected would contain similar non  $\alpha$ -helical conformations by slow evaporation of a  $40$  °C AP solution (at  $40$  °C, low concentration AP is mainly in a PPII conformation<sup>35,36,66</sup>).

Figure 10 compares the spectra of the solid AP samples prepared by these two methods to the  $70$  °C solution  $\beta$ -sheet spectrum of a 1:1 molar mixture of polyglutamic acid (PGA) and polylysine (PLL), and to solution spectra of AP at various temperatures. The PGA-PLL spectrum

shown is a calculated pure  $\beta$ -sheet spectrum where contributions from other conformations have been numerically removed.<sup>67</sup>

The high temperature, evaporated solid AP spectrum is roughly similar to the  $\beta$ -sheet spectrum. For example, the Am I bands occur at  $\sim 1670\text{ cm}^{-1}$  (the increased AmI band intensity in AP and the  $\sim 1690\text{ cm}^{-1}$  shoulder results from arg sidechain contributions which are absent in the PGA-PLL sample). Similar AmII frequencies occur in the evaporated AP and  $\beta$ -sheet spectra, although the bandshapes show differences. A higher AmIII frequency occurs in the evaporated AP spectrum than in the PGA-PLL  $\beta$ -sheet spectrum. These differences probably result from the existence of additional conformations in the evaporated AP sample.

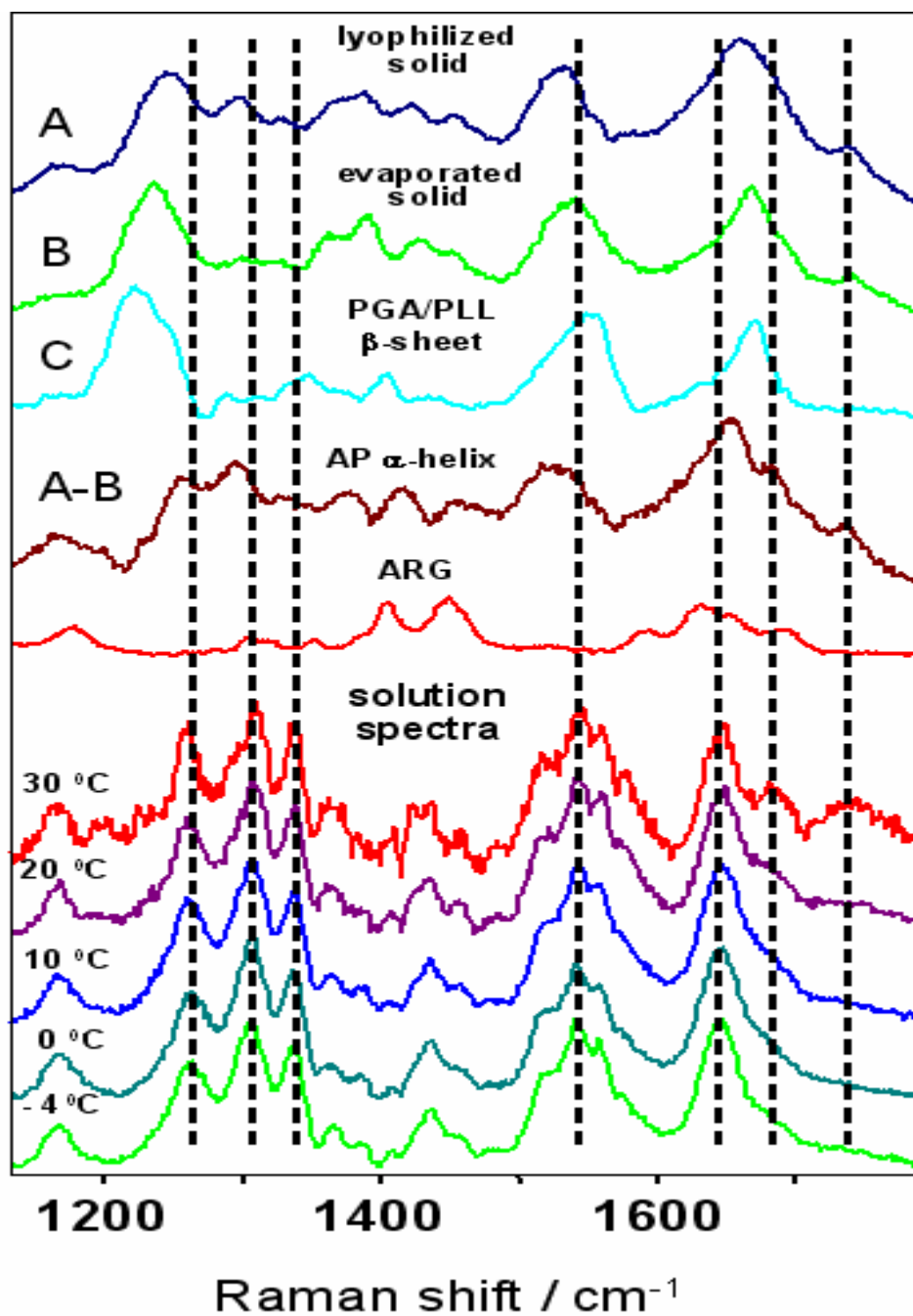


**Figure 10.** 204 nm UV resonance Raman spectra of A: solid sample obtained by freezing a -5 °C AP solution and lyophilizing (~63 %  $\alpha$ -helix). B: solid sample obtained by evaporating 40 °C AP solution. C: calculated spectrum of pure  $\beta$ -sheet PGA-PLL stoichiometric mixture in solution at 70 °C. A-B: solid AP  $\alpha$ -helix spectrum calculated by subtracting spectrum B from spectrum A. Lower spectra are pure  $\alpha$ -helix AP solution spectra at the indicated temperatures.

We calculated the solid  $\alpha$ -helix spectrum from the  $-5$  °C liquid nitrogen frozen lyophilized AP sample by subtracting an appropriate amount of the evaporated AP spectrum. This yielded a spectrum similar in shape to those of the  $\alpha$ -helix solution spectra shown at the bottom of Figure 10. These  $\alpha$ -helix solution spectra were calculated by subtracting appropriate amounts of PPII conformation spectra from the measured spectra, as described previously.<sup>36,64</sup>

The 204 nm UVRS AP solution phase  $\alpha$ -helical spectra are distinguished by a triplet of AmIII bands [labeled AmIII<sub>1</sub> ( $1337\text{ cm}^{-1}$ ), AmIII<sub>2</sub> ( $1306\text{ cm}^{-1}$ ), and AmIII<sub>3</sub> ( $1261\text{ cm}^{-1}$ ) at  $-4$  °C]<sup>64</sup> and the absence of a  $\sim 1400\text{ cm}^{-1}$  C $\alpha$ -H bending band. The AmII band occurs at  $1542\text{ cm}^{-1}$ , while the AmI band occurs at  $1647\text{ cm}^{-1}$ . Peptides in which the amide bonds are hydrogen bonded to water show major downshifts for the AmII and AmIII bands, and upshifts for the AmI band when the temperature increases due to weakening of water hydrogen bonding.<sup>19,60,64</sup> In contrast, few changes occur for the solution phase  $\alpha$ -helix conformation, where most of the hydrogen bonding is satisfied by intramolecular interactions. Only the AmIII<sub>3</sub> band shows a significant frequency decrease with temperature.

The calculated 204 nm UVRS of solid  $\alpha$ -helical AP is similarly dominated by a triplet of AmIII bands, which are all downshifted from that in solution. Compared to the  $-4$  °C solution spectrum the solid  $\alpha$ -helix AmIII<sub>1</sub> band downshifts  $3\text{ cm}^{-1}$ , while the AmIII<sub>2</sub> band downshifts  $11\text{ cm}^{-1}$  and the AmIII<sub>3</sub> band downshifts  $5\text{ cm}^{-1}$ . Thus, removal of water hydrogen bonding decreases the AmIII triplet frequencies much more than does the modest temperature induced weakening of the water hydrogen bond strengths.

Both the AmII and AmIII bands, which are admixtures of C-N stretching and N-H bending, upshift as hydrogen bonding to the amide bond increases. This upshift occurs for two reasons: a water molecule hydrogen bonded to the amide hydrogen increases the N-H bending

force constant, and hydrogen bonding stabilizes a resonance structure which increases the double bond character of the C=N bond.<sup>19,35</sup> Thus, these vibrational frequencies increase.

The AmII band at 1524 cm<sup>-1</sup> shows the largest frequency decrease (20 cm<sup>-1</sup>) upon the loss of water hydrogen bonding. This behavior is similar to that previously observed for the temperature dependence of the PPII conformation.<sup>35,36</sup> The AmII vibration is the most sensitive to hydration according to Torii *et al's*<sup>68</sup> theoretical N-methylacetamide calculations.

In contrast, the AmI band peak at 1652 cm<sup>-1</sup> is frequency upshifted by 7 cm<sup>-1</sup> compared to  $\alpha$ -helical AP in water due to a loss of water hydrogen bonding. This AmI band upshift is expected due to increased contribution of the carbonyl double bonded resonance structure.<sup>19,35</sup> In addition, another band appears in solid  $\alpha$ -helix AP at ~1734 cm<sup>-1</sup> which also emerges in  $\alpha$ -helix AP in water at the highest temperature of 30 °C. This 1734 cm<sup>-1</sup> band probably derives from a non hydrogen bonded amide C=O groups.

This study allows us to conclude that a hydrogen bonding water sheath occurs around a polyalanine  $\alpha$ -helical peptide. This peptide-water hydrogen bonds increase the AmII and AmIII band frequencies and decrease the AmI frequency. We can use this correlation to monitor hydrogen bonding of  $\alpha$ -helices in proteins. As shown elsewhere<sup>60,64,69</sup> we can isotopically edit particular peptide bonds to determine amide band frequencies for particular bonds to determine hydrogen bonding at particular sites.

### **3.0 POLY(N-ISOPROPYLACRYLAMIDE) VOLUME PHASE TRANSITION.**

#### **3.1 INTRODUCTION**

Proteins exhibit a maximum conformational stability in a narrow temperature range usually centered around their host operating temperature.<sup>70-72</sup> Outside of this range the native state is destabilized and may denature. The denaturation that occurs with temperature increases is generally ascribed as resulting from the increased contribution to the free energy of the entropy term. In contrast, the cold denaturation that occurs as the temperature decreases has a more complex origin. Although it occurs for essentially all proteins, this cold denaturation is less recognized, because it often only becomes clearly evident at temperatures below the freezing point of water

It is well known that around room temperature hydrocarbon solubility decreases with temperature.<sup>11,73</sup> Since most native state proteins compartmentalize their hydrophobic residues leaving hydrophilic groups on the protein surface, lowering the temperature should destabilize the native state. When proteins fold back from being heat or cold denatured they will undergo a hydrophobic collapse where non-polar residues bury themselves inside of the molten globules leaving polar groups exposed to water. Although there are lots of arguments to explain these phenomena, which invoke hydrophobic forces, there remains some residual vagueness to the arguments. A clear characterization of the molecular changes that occur is needed.

The protein cold denaturation mechanism can be studied on a synthetic polymer poly(N-isopropylacrylamide) (PNIPAM) which has a similar transition. PNIPAM is one of the first and best examples of a reversible hydrogel volume phase transition<sup>74,75</sup> which is driven by temperature changes. It has been suggested that below the transition temperature, which is referred to as Lower Critical Solution Temperature (LCST), amide-water hydrogen bonding forces dominate, and the polymer exists in an extended coil-like conformation. These arguments proclaim that at temperatures above the LCST, hydrophobic interactions start to prevail and the coil state collapses into a compact globule in order to minimize polymer-water contacts.

The volume phase transition is analogous to the phenomenon of cold denaturation<sup>76-80</sup> especially if the PNIPAM occurs in the form of nanogel particles. Weissman *et al.*<sup>81</sup> has showed that a colloidal dispersion of monodisperse ~300 nm nanogel PNIPAM particles (~3 % polymer and contained 97 % water at 15 °C) reversibly collapses to 100 nm pure polymer spheres by a temperature of 35 °C. Figures 11 and 12 show views of NIPAM solution at different temperatures while Figure 13 shows schematic representation of the transition.



**Figure 11.** Transparent NIPAM solution at 25 °C. Swollen particles, ~ 200 nm diameter.



**Figure 12.** Turbid NIPAM solution at 45 °C. Collapsed particles, ~ 50 nm diameter.

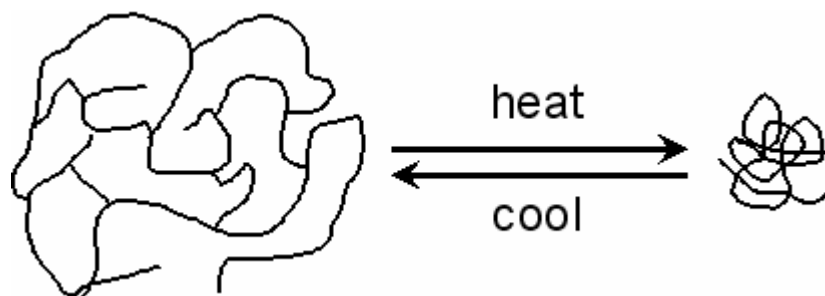


**Figure 13.** Schematic representation of the transition.

The phenomenon of volume phase transition in NIPAM has been known since 1960s.<sup>82</sup> Until 1990s it has been studied mostly by calorimetry, light scattering, viscometry and fluorescence (see references in a review by Schild<sup>82</sup>). Experimental and theoretical studies on both single chain polymer and gels created a model which describes the transition as dehydration of polymer chains which may be followed by aggregation and phase separation. In the last two decades spectroscopic techniques were also applied to study the phenomenon.

Comprehensive vibrational analysis of NIPAM was performed by Maeda *et al* using FTIR spectroscopy.<sup>83-89</sup> Authors observed characteristic changes in vibrations of both

hydrophobic and hydrophilic moieties of the polymer during the phase transition and attributed them to dehydration of the polymer at high temperature. Lin *et al.*<sup>90</sup> made similar observations by applying micro-attenuated total reflection/FTIR to microgel samples. The authors indicated change in both intramolecular hydrogen bonding and hydrophobic interaction during the gel collapse. Katsumoto *et al* offered an alternative band assignment of the carbonyl vibrations.<sup>91-95</sup> Authors studied local structure of the polymer chains during the NIPAM phase transition using attenuated total reflection/infrared spectroscopy. (ATR/FTIR) They ascribed a lower wavenumber component of Amide I peak to intramolecular C=O – H-N hydrogen bonding species in the polymer. Authors proposed that spectral changes during the transition indicate disruption of these intramolecular hydrogen bonds in the polymer. Another group<sup>96</sup> utilizing ATR/FTIR attributed spectral changes to breaking of intermolecular hydrogen bonds, and formation of intramolecular hydrogen bonds between free amides. The authors did not report changes in hydrophobic group vibrations.

Several authors suggest that property of water is a key factor in the phase transition process. Annaka *et al* used low frequency Raman scattering<sup>97</sup> and OH stretching vibration of water<sup>98</sup> to study effects of salts on NIPAM phase transition. Authors point out that chemical potential of water determines hydration of NIPAM. Presence of ions disrupts water hydrogen bonding network surrounding NIPAM hydrophobic groups, which reduces hydrophobic hydration and causes the gel to collapse. Suzuki *et al* used the same technique<sup>99</sup> to suggest that gel collapse is induced by destruction of tetrahedral structure of water. Terada *et al.*<sup>100</sup> studied structure of water around NIPAM by Raman spectroscopy. They proposed that small water domains are included in polymer (so-called interstitial water) and water inside of these domains have different spectral characteristics. Appel *et al.* used Raman microimaging to study structure

of the gel based on CH<sub>2</sub> bending band.<sup>101,102</sup> Authors conclude that pores of water rich phase exist among polymer segments at low temperatures. According to authors, these pores diminish in size as temperature increases and become unresolvable at phase transition temperature and above.

In several studies authors force the polymer to undergo the transition by other than temperature stimuli. Meersman *et al.* studied pressure induced phase transition in NIPAM by FT/IR.<sup>79</sup> Spectral analysis showed that increase in pressure causes increased hydration of the polymer, which confirms with higher values of the transition temperature at higher pressure. Tsuboi *et al.*<sup>103</sup> developed a confocal Raman microspectroscopy and employed it to observe polymer particles created by radiation pressure. Authors characterized different states of the polymer in a wide wavenumber region (800-3500 cm<sup>-1</sup>). Structure of particles created by radiation pressure was similar to collapsed state of the polymer.

There are reports on rather unusual interpretation of the phase transition. For example, Wu *et al.* utilized 2D correlation IR spectroscopy for study temperature and pressure induced NIPAM phase transitions.<sup>104</sup> Authors saw small irreversible changes in Amide I peak which are not seen in one dimensional technique. Zeng *et al.* used IR and Raman spectroscopy to characterize samples obtained by drying polymer at either coiled or collapsed state.<sup>105</sup> Authors suggest that *trans*- to *cis*- isomerization of amide group occurs during the polymer collapse.

In spite of ambiguity among researchers in interpretation of spectral changes, the general understanding of the transition is that the transition between two states results from a balance between amide groups hydrogen bonding to water and hydrophobic hydration of isopropyl groups.<sup>74,75,98,106-111</sup>

## 3.2 EXPERIMENTAL

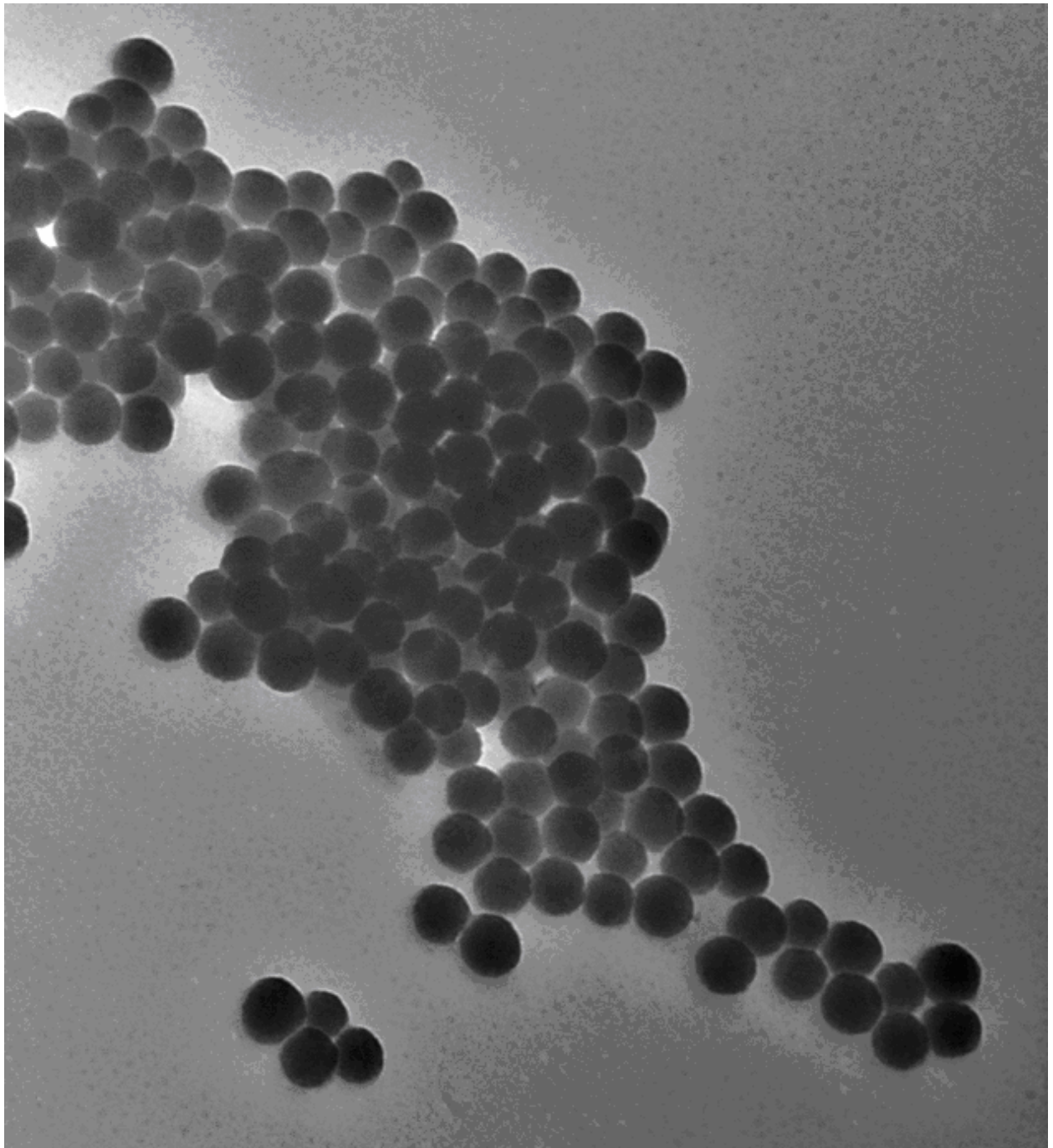
### 3.2.1 Sample preparation.

We prepared ~100 nm particles of NIPAM and NIPAM-d<sub>7</sub> via emulsion polymerization as follows: ~200 mg of N-isopropylacrylamide was dissolved in 1 ml of deionized water. To this solution ~10 mg of N,N-methylene-bisacrylamide and ~2 mg of 2-acrylamido-2-methyl-1-propanesulfonic acid were added. The resulting solution was purged with nitrogen for 15 min and then transferred into 15 ml of 0.06 % sodium dodecyl sulphate solution at 50 °C. The solution temperature was then raised to 70 °C and 0.2 ml of 0.04 % ammonium persulphate solution (initiator) was added. After stirring for 2 hr at 70 °C the reaction mixture was cooled to room temperature and dialyzed against deionized water in SnakeSkin<sup>TM</sup> dialysis tubing (10,000 MWCO) to wash away dodecyl sulphate, unreacted monomers and single chains. Washing continued for 2 weeks with daily change of water. Sample of NIPAM-d<sub>7</sub> was prepared by an analogous procedure using N-isopropyl-d<sub>7</sub>-acrylamide. Particle size was measured by dynamic light scattering and transmission electron microscopy (TEM). The TEM images were obtained by using FEI Morgagni 268 microscope system with a typical magnification of 18,000×. Samples were prepared by placing a droplet of solution on the grid and removing the liquid in 15 min with a soft tissue. The polydispersity of samples was less than 20 %. A typical TEM image is shown in Figure 14.

### 3.2.2 Instrumentation.

The UV Raman instrumentation has been described in detail elsewhere.<sup>36,66,112</sup> Briefly, a Coherent Infinity Nd:YAG laser was used to produce a 355 nm (3rd harmonic) beam which was then Raman-shifted to 204 nm (5th anti-Stokes) by using a 1-m tube filled with H<sub>2</sub> gas at 60 psi. The 204 nm beam was selected with a Pellin Broca prism, and focused on a sample which was circulated in a thermostated free surface flow stream. The Raman scattered light was imaged into a subtractive double spectrometer and detected by a Roper Scientific Spec-10:400B liquid nitrogen cooled CCD camera.

Kinetic experiments utilized 2 synchronized Nd:YAG lasers, one of which produced a 1.9  $\mu\text{m}$  IR heating pulse while the other produced probe pulse at either 204 nm (see above) or 532 nm (second YAG harmonics) with delay times ranging between 0.02 and 100  $\mu\text{s}$ . The 1.9  $\mu\text{m}$  beam was obtained by Raman shifting 1.06  $\mu\text{m}$  fundamental of Nd:YAG laser (1st H<sub>2</sub> Stokes) in a 1-m tube (Light Age, Inc) filled with H<sub>2</sub> at 1000 psi. The magnitude of the T-jump was measured by using the  $\sim 3300\text{ cm}^{-1}$  temperature dependent water O-H stretching bands.<sup>36,66,113,114</sup> Initial temperature of the NIPAM solution was kept at 30 °C, a few degrees below the phase transition temperature. Under this experimental conditions absorption of the 1.9  $\mu\text{m}$  pulse led to  $\sim 25\text{ }^\circ\text{C}$  temperature increase. Thus, the temperature of a heated sample is around 55 °C, the highest temperature at which the steady state spectra were measured.



1e.jpg  
Print Mag: 86000x @ 7. in  
14:26 05/16/05

100 nm  
HV=80kV  
Direct Mag: 44000x  
X: Y:  
Microscopy Facility

Figure 14. TEM image of PNIPAM particles.

The 488 nm excited Raman spectra were collected using the following setup. A Coherent INOVA 90C Ar<sup>+</sup> ion laser produced 488 nm light, which was passing through a 488 nm narrow band interference filter (CVI Laser, LLC) and focused on a sample in a thermostated free surface flow stream. The Raman scattered light was imaged into a single spectrometer. A holographic notch filter (Kaiser Optical Systems, Inc) was used to reject the Rayleigh light. Spectra were detected by a Roper Scientific Spec-10:400B liquid nitrogen cooled CCD camera.

### 3.3 RESULTS AND DISCUSSION.

The phase transition of NIPAM single chain in solution is usually described as coil to globule transition followed by aggregation.<sup>83,85,115</sup> In case of nanogel particles the transition consists of expulsion of water from particles during which they contract. Consequently, solvent exposure of the particle interior will change, and new specific mutual orientation of functional groups will be established.

The temperature of the microgel transition may differ from that of the single chain polymer and is typically around 35 °C. The simplest experimental way to determine the phase transition temperature is by monitoring the cloud point. Swollen particles scatter light less efficiently than collapsed ones,<sup>81,116</sup> and solution is almost transparent at temperatures below the transition point. As particles shrink, their dielectric constant becomes much different from that of water, and solution turns opaque. Figure 15 shows change of solution turbidity at 500 nm with temperature on NIPAM sample. The solution becomes visibly cloudy at temperatures above 30 °C. The transition is not as sharp as that of single chains in solution.<sup>115</sup> The saturation value of turbidity is not reached until 50 °C, indicating that particles are still undergoing some change

below 50 °C. The transition temperature of this sample determined by inflection point of the turbidity-temperature curve is around 37 °C. In this study we monitor structural and environmental changes occurring with microgel particles during this process.

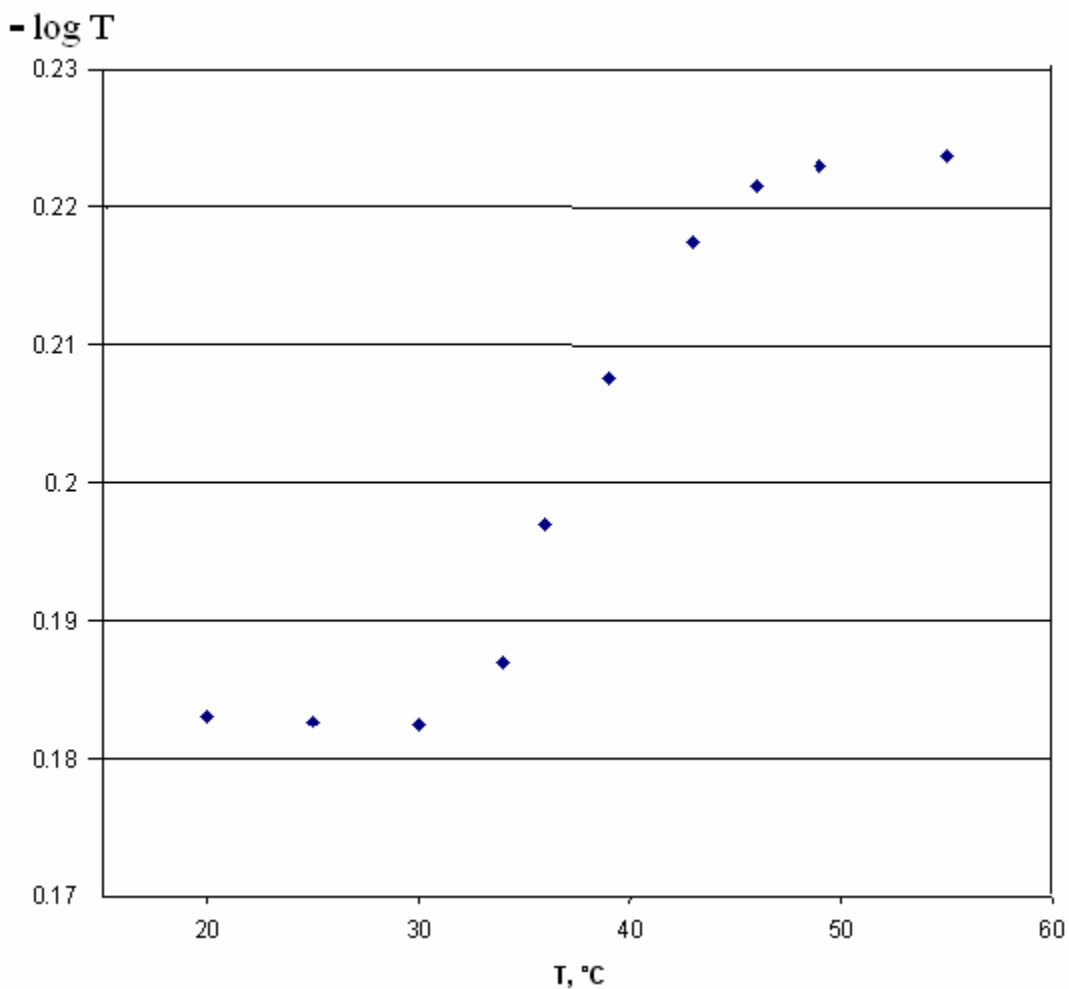
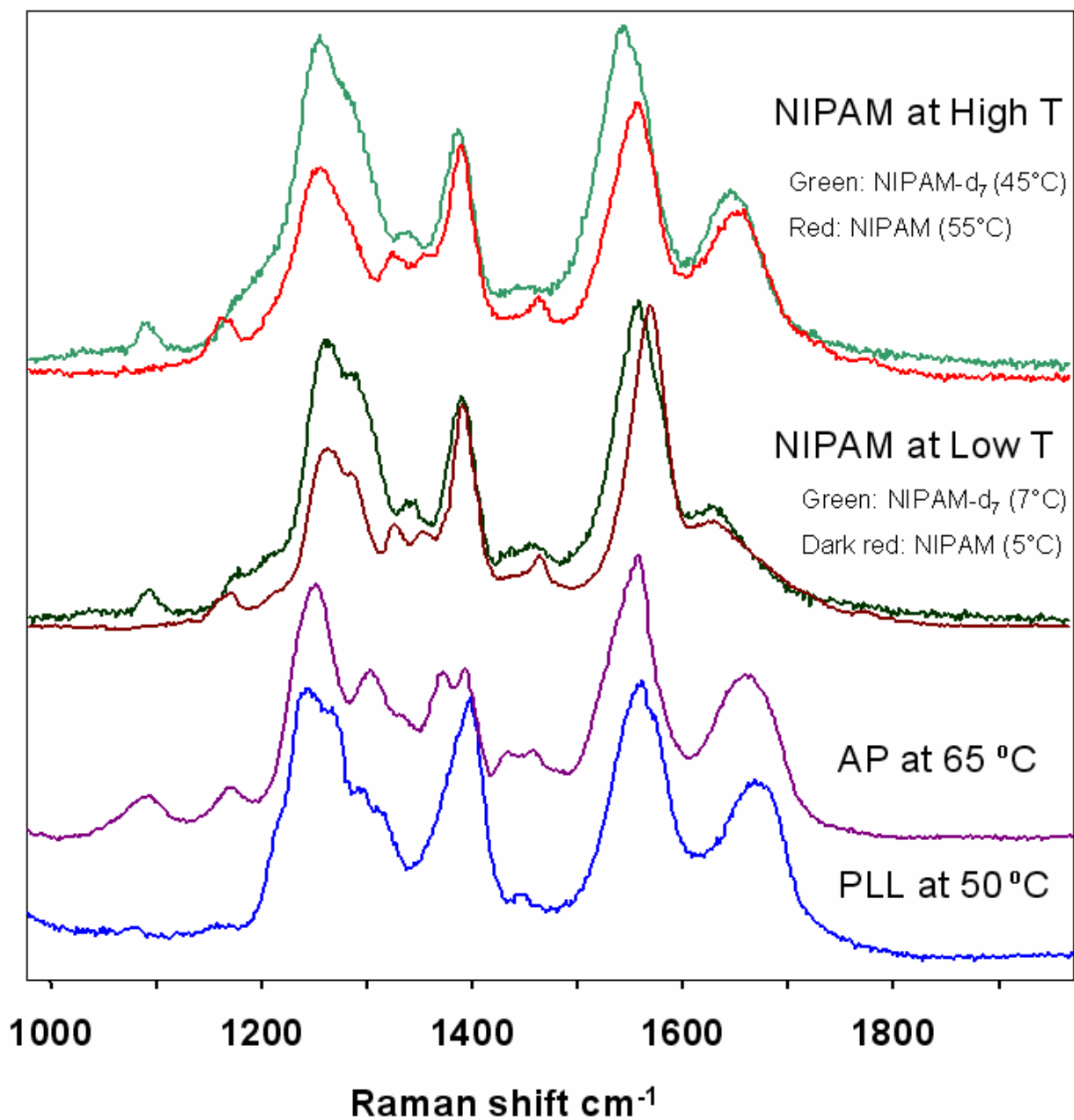


Figure 15. Turbidity of NIPAM solution measures ad 500 nm.

### 3.3.1 UV Raman Spectra. Amide Region.

We obtained 204 nm excited UV Raman (UVR) spectra of aqueous solutions of NIPAM and NIPAM-d<sub>7</sub>. The 204 nm UVR spectra of aqueous solutions of NIPAM and NIPAM-d<sub>7</sub> are similar to each other and to spectra of model peptides in extended conformations. Figure 16

shows spectra of NIPAM and NIPAM-d<sub>7</sub> at high and low temperatures (which correspond to states before and after transition) as well as spectra of poly-L-lysine and alanine peptide (AP, 21-mer containing 3 Arg and 18 Ala residues) at high temperatures. Spectra of all compounds are dominated by four major bands that in case of NIPAM occur at the following frequencies: AmI (~1630 cm<sup>-1</sup>), AmII (~1550 cm<sup>-1</sup>), C-H bending (~1380 cm<sup>-1</sup>), and AmIII (~1260 cm<sup>-1</sup>). The appearance of these bands is determined by a NIPAM unit that contains the peptide bond. Figure 17 shows structures of NIPAM and its deuterated derivative with peptide bond unit highlighted. Also, possible rotations that determine orientation of the pendant group in space are shown by arrows.



**Figure 16. 204 nm excited UV Raman spectra of NIPAM and NIPAM-d<sub>7</sub> at temperatures below and above the transition, as well as the spectra of AP and PLL.**

Since NIPAM contains structural unit similar to that of peptides, excitation at 204 nm yields spectra dominated by vibrations of peptide group: C-N, C-C, and C=O stretch, as well as

N-H and C-H bending.<sup>49</sup> Extensive studies on model peptides show that positions of spectral bands depend on mutual orientation of atoms in space and their environment.<sup>117-120</sup>

Comparing spectra of NIPAM and NIPAM-d<sub>7</sub> one can see that relative intensities of bands are different in these two samples. In NIPAM-d<sub>7</sub> the AmIII band is more intense comparing to AmI and C-H<sub>b</sub> bands. This difference could be explained by the fact that AmIII bands have contribution of N-C<sub>isopropyl</sub> stretching vibration which is coupled to some extent to C-H bending motion of adjacent methine group. Upon deuteration this coupling disappears which may lead to higher magnitude of N-C<sub>isopropyl</sub> vibration. Thus, intensity of resonance enhanced band increases.

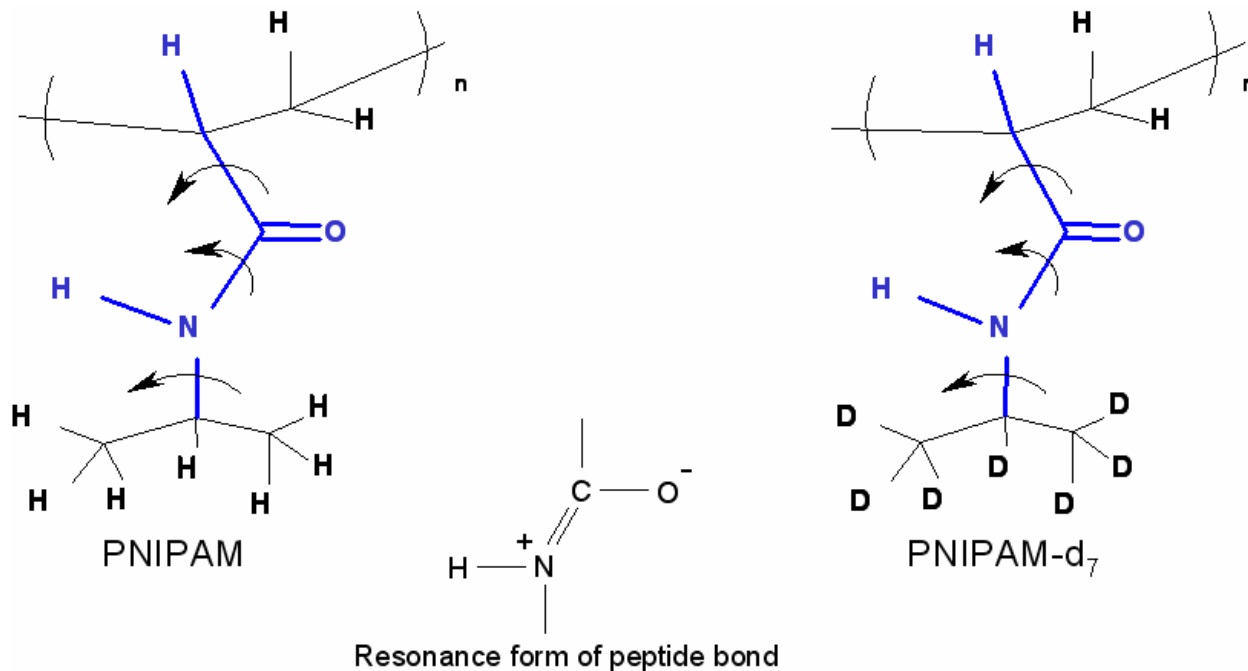


Figure 17. Repeat unit of poly(N-isopropylacrylamide chain)

### 3.3.1.1 AmIII

The AmIII band is the most sensitive to a change in peptide conformation, in particular to peptide  $\psi$  angle.<sup>117,121</sup> It corresponds to bending vibrations of N-H bond coupled in phase to C-N stretching vibrations. Figure 18 shows temperature dependence of 204 nm UVR spectra of NIPAM. There are 2 bands in the AmIII region. At lowest temperature they are clearly resolved and show up at 1258  $\text{cm}^{-1}$  and 1289  $\text{cm}^{-1}$ . As temperature rises, 1289  $\text{cm}^{-1}$  peak gradually becomes less prominent, until it almost disappears at 55 °C. Only non-symmetrical shape of the band indicated existence of second component underneath the broad peak. In the temperature interval from 5 to 35 °C the 1258  $\text{cm}^{-1}$  band moves about 3  $\text{cm}^{-1}$  to 1255  $\text{cm}^{-1}$ , which is similar to temperature dependence of a polypeptide in the extended conformation.<sup>35,36</sup> Such temperature dependence is consistent with gradual weakening of water to amide hydrogen bonding as temperature rises. Upon further heating the band downshifts additional 5  $\text{cm}^{-1}$  over 20 °C which can not be attributed to the same process. Shift of such magnitude is more likely attributable to rotations of the amide group around one (or several) of the angles indicated in Figure 17. It may also correspond to drastic change in the environment around the group.

The 1289  $\text{cm}^{-1}$  band, on the other hand, does not experience such a large shift, it moves about 2.5  $\text{cm}^{-1}$  over 30 °C before the transition, and another 2.5  $\text{cm}^{-1}$  over 20 °C after beginning of the transition. Such band shift is consistent with temperature dependence due to weakening of hydrogen bonding to water. This behavior is possible if the 1289  $\text{cm}^{-1}$  band has different normal mode composition which is less sensitive to three-dimensional orientation of the peptide group.

The temperature dependence of the NIPAM-d<sub>7</sub> aqueous solution is similar to that of NIPAM sample, as shown in Figure 19. There is little difference in spectra at 7, 16 and 33 °C. Spectrum at 45 °C, however, demonstrates upshift of the AmI band from 1627 to 1645  $\text{cm}^{-1}$  and

downshift of the AmIII band from 1262 to 1254  $\text{cm}^{-1}$ . A low wave number shoulder appears on the AmII as well. Similar behavior of the NIPAM-d<sub>7</sub> supports a hypothesis that isopropyl group does not influence much the amide spectra in both swollen and collapsed states.

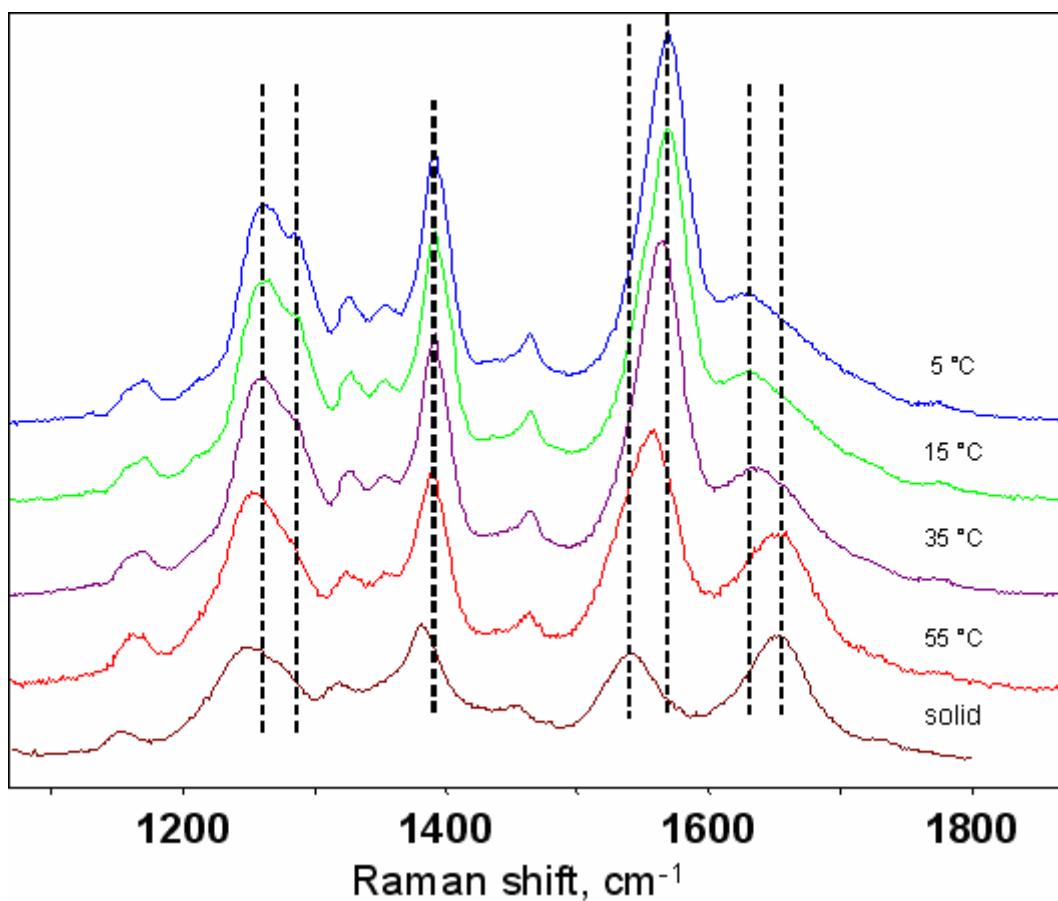


**Figure 18.** Temperature dependence of PNIPAM aqueous solution amide spectra

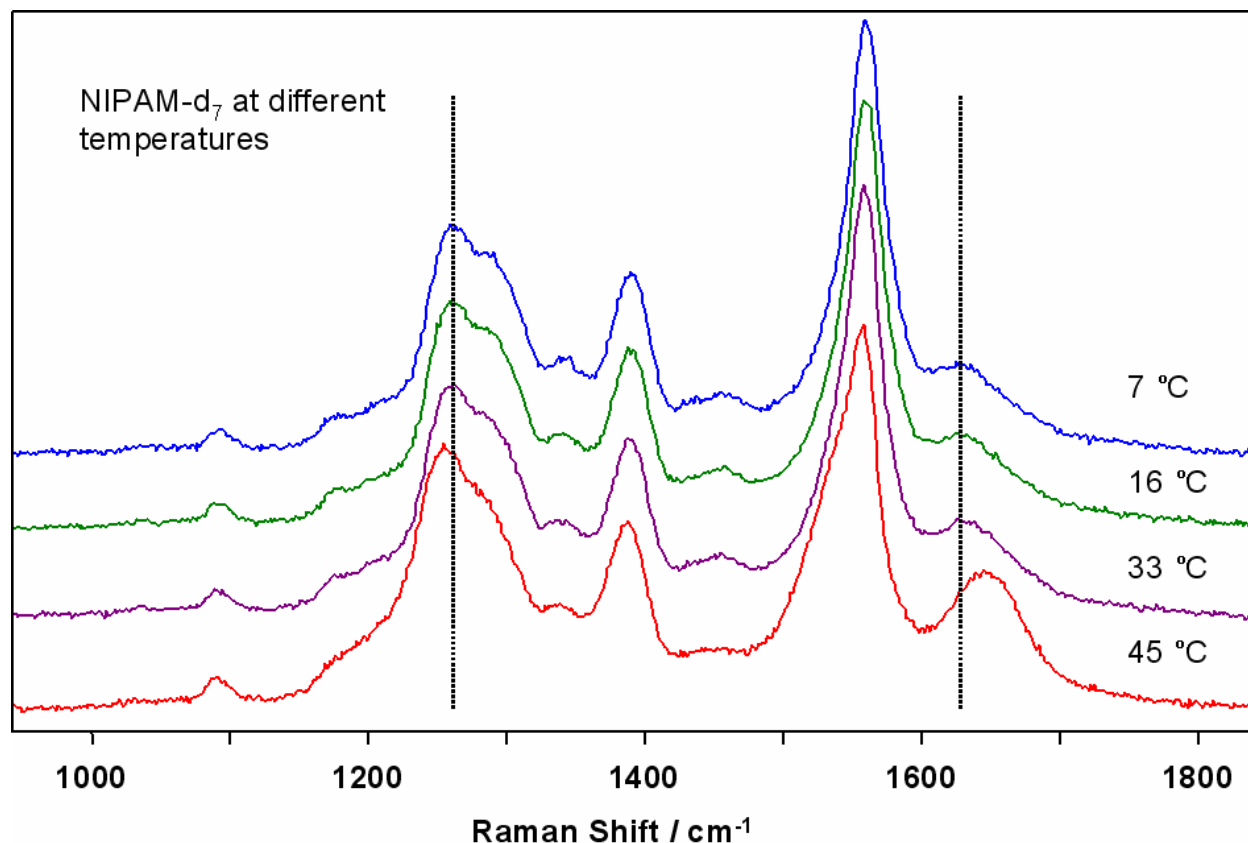


Figure 19. Temperature dependence of NIPAM-d<sub>7</sub> sample in water.

### 3.3.1.2 C-H<sub>b</sub>

Several conclusions can be reached based on the C-H bending band at  $\sim 1380 \text{ cm}^{-1}$ . First, its appearance in both NIPAM and NIPAM-d<sub>7</sub> signifies that this band corresponds to a C-H bending vibration of a methine group in the main chain (Figure 17). Further, its relative intensity suggests, that conformation of peptide unit in NIPAM is similar to that of peptide group in polypeptides in an extended conformation. The emergence of this band suggests mutual orientation of C-H and N-H bonds in which bending motions of these two hydrogen atoms are coupled. This coupling provides resonance enhancement to C-H<sub>b</sub> vibration<sup>117</sup>.

The C-N and C=O bonds of the peptide unit in reality have partial double character as a result of existence of resonance structure shown in Figure 17. Such bond character prevents

rotation around C-N bond, so that OCNH dihedral angle exists at fixed position around  $180^\circ$ . Such *trans*- configuration of peptide bond is common for most polypeptides and proteins, since it is energetically more favorable than the other possible *cis*- form with OCNH angle  $0^\circ$ . The *trans*- configuration of peptide bond in NIPAM is supported by the AmII and AmIII peak positions, that are similar to that of peptide in *trans*- configuration and by the absence of bands pertaining to *cis*- configuration.<sup>122-125</sup> As Figure 16 shows, no drastic changes occur for AmIII, AmII, and C-H<sub>b</sub> bands at higher temperatures, meaning that the *trans*- configuration of a peptide bond is preserved during the transition, in contrary to the mechanism proposed by Zeng *et al.*<sup>105</sup> The authors observed different intensity of C-H stretching and bending bands in samples prepared by drying before and after the phase separation. They argue that CH<sub>3</sub> asymmetric stretching vibration is more intense in *cis*- than in *trans*- isomer.

### 3.3.1.3 AmII.

The AmII band of polypeptides has the biggest temperature dependence of all amide bands.<sup>35,36</sup> In NIPAM it is also shows a pronounced shift. Overall AmII envelope downshifts about  $4\text{ cm}^{-1}$  in the interval from 5 to 35 °C, and then  $\sim 15\text{ cm}^{-1}$  over 20 °C interval after the onset of the transition. The AmII band of  $\alpha$ -helical peptide is also highly sensitive to hydration state.<sup>119</sup> Thus, such a large bandshifts of NIPAM AmII is expected, since phase transition consists of dehydration of microgel particles.

Spectral deconvolution of the AmII bands shows two AmII components with different behavior. At 5 °C they are centered at 1549 and  $1569\text{ cm}^{-1}$  respectively. Low wavenumber component is highly sensitive to dehydration occurring during particle collapse. Between 35 and 55 °C it downshifts  $19\text{ cm}^{-1}$  and remains on the same position in the solid. Higher wavenumber component is not as sensitive to a collapse ( $5\text{ cm}^{-1}$  shift from 35 to 55 °C) but highly susceptible

to changes which occur after that. The band of this component downshifts  $15\text{ cm}^{-1}$  between  $55\text{ }^{\circ}\text{C}$  solution and the solid state. The AmII position at  $55\text{ }^{\circ}\text{C}$  suggests that the particles are partially hydrated at this temperature as compared to a solid sample.

#### **3.3.1.4 AmI.**

The AmI band experiences the most drastic change upon phase transition. The band corresponds to a normal mode which is mostly a C=O stretch.<sup>85</sup> It is known, that water molecule hydrogen bonded to carbonyl oxygen downshifts the AmI peak frequency. Therefore, dehydration will be accompanied by the upshift of the band, in contrast to the behavior of the AmII and AmIII bands. Spectral deconvolution of the AmI region shows that there are at least two bands underneath the peak with frequencies about  $1630\text{ cm}^{-1}$  and  $1670\text{ cm}^{-1}$ . It has been proposed<sup>83</sup> that a lower wavenumber peak corresponds to a hydrated carbonyl, while higher wavenumber component is due to a non-hydrated (“free”) carbonyl. The ratio of intensities of these two components can serve as a measure of carbonyl hydration.

Figures 20-22 demonstrate spectral modeling of this region for temperatures 15, 35 and  $55\text{ }^{\circ}\text{C}$ . In order to achieve satisfactory modeling, components of the AmI peak were allowed to vary within  $1625\text{-}1635\text{ cm}^{-1}$  and  $1665\text{-}1675\text{ cm}^{-1}$  intervals respectively. At temperatures up to  $35\text{ }^{\circ}\text{C}$  little change occurs with AmI band, only slight intensity increase of  $\sim 1670\text{ cm}^{-1}$  component. However, drastic change takes place at  $55\text{ }^{\circ}\text{C}$ . Not only intensity ratio of  $1670\text{ cm}^{-1}$  to  $1630\text{ cm}^{-1}$  significantly increases (from 0.65 at  $35\text{ }^{\circ}\text{C}$  to 1.8 at  $55\text{ }^{\circ}\text{C}$ ), but also the overall AmI band intensity becomes higher comparing to other bands. The band shape at  $55\text{ }^{\circ}\text{C}$  is similar to that of a solid sample, relative intensity of AmI band is even higher in the solid. Such AmI intensity increase upon dehydration was not observed in peptides,<sup>119</sup> but it is similar to behavior of N-methylacetamide (NMA) in dry acetonitrile comparing to that in water.<sup>126,127</sup> Figure 23 shows

change in intensity of the AmI band components with temperature comparing to turbidity of the sample.

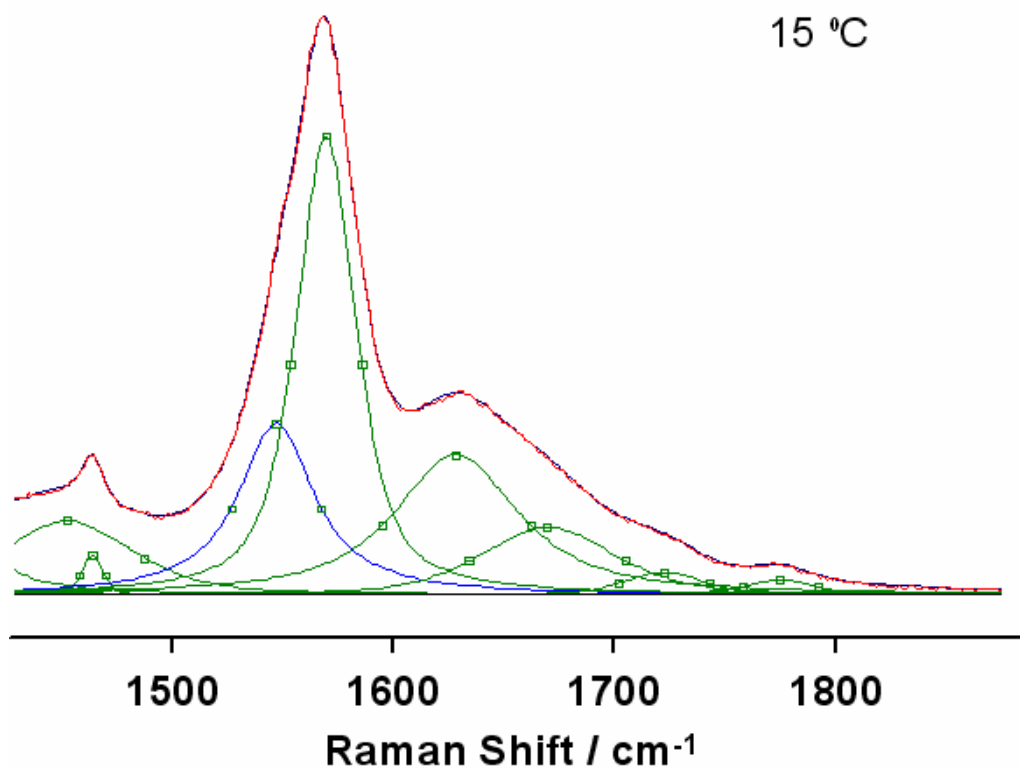


**Figure 20.** Modeling of the AmI and AmII spectral region for 15 °C spectrum of NIPAM.

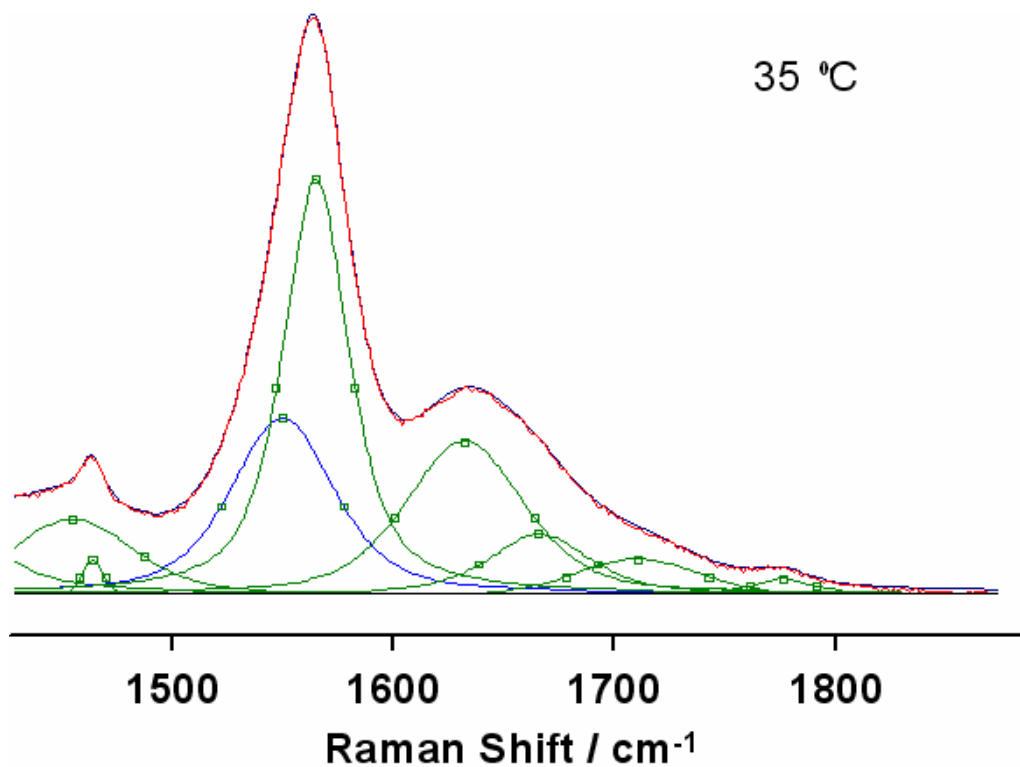


**Figure 21.** Modeling of the AmI and AmII spectral region for 35 °C spectrum of NIPAM.

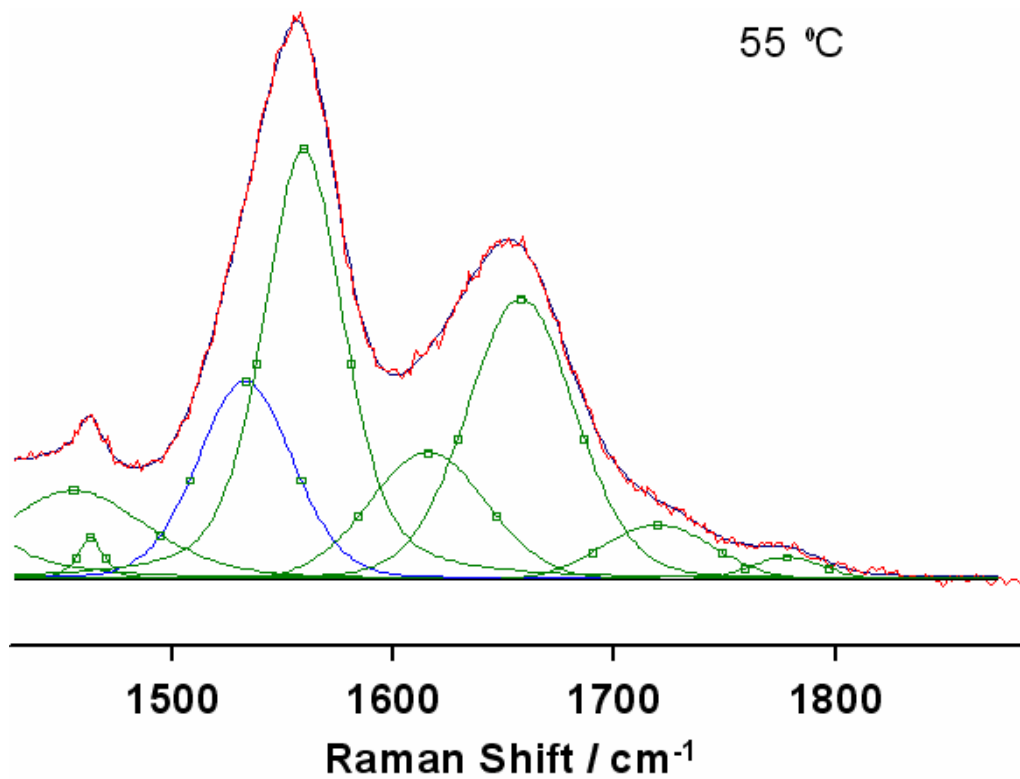


**Figure 22.** Modeling of the AmI and AmII spectral region for 55 °C spectrum of NIPAM.

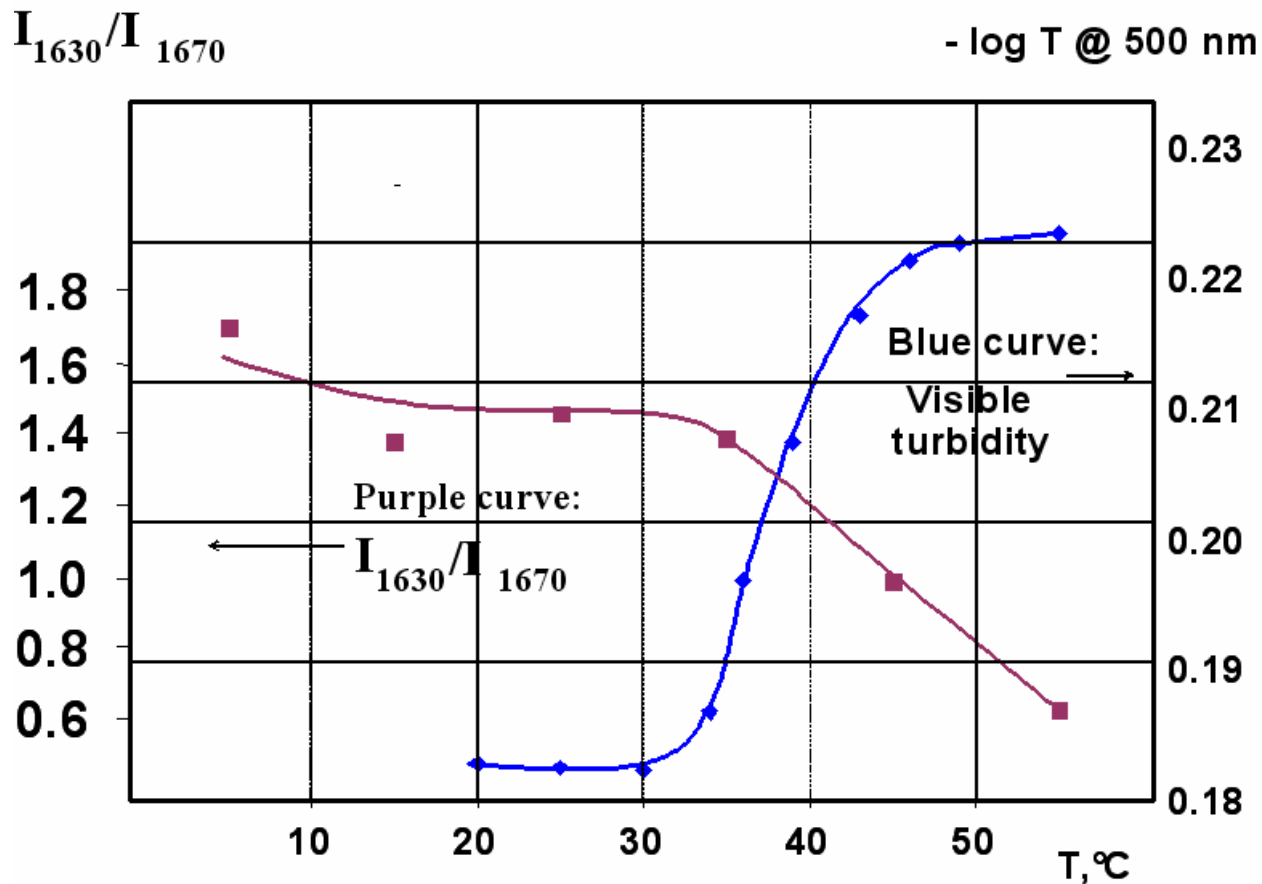


Figure 23. Intensity ratio of the AmI band components comparing to turbidity.

Since peptide group of NIPAM is not incorporated into the main chain of the polymer, its behavior is more similar to that of NMA, than polypeptide. The AmI intensity increase of NMA in dry acetonitrile comparing to that of NMA in water may be due to differences in carbonyl excited state geometry in these two solvents.<sup>127</sup> According to calculations,<sup>127</sup> excited state of NMA in acetonitrile has more elongated C=O bond than that in water. Alternative explanation is that carbonyl bond length of aqueous ground state is larger due to hydrogen bonding to water which decreases the net displacement.<sup>126</sup> Both these scenario result in higher intensity of the AmI band. Since NIPAM transition consists of dehydration of particles, the carbonyl groups are

expected to be in less hydrogen bonding environment after the collapse causing the AmI intensity increase by a similar mechanism.

The spectrum of a solid sample is similar to a 55 °C solution spectrum. The AmI and AmIII bands show up at roughly the same positions with similar band shapes. The AmII band downshifts 15  $\text{cm}^{-1}$  which is consistent with its high sensitivity to hydration. The C-H<sub>b</sub> band downshifts  $\sim 7 \text{ cm}^{-1}$  in the solid which could result from rotation of pendant group with respect to the main chain in order to adopt close neighboring of different particles.

The AmI band can be modeled with only one peak, which position changes with temperature. Such modeling of the phase transition, is shown figure 24 comparing to the AmIII band and particle size. A change in the AmIII position almost coincides with change in size. The midpoint of the transition is around the same temperature ( $\sim 32 \text{ }^\circ\text{C}$ ) for both curves. Steepness and curvature of the curves are similar as well. The changes in the AmI peak, however, occur at longer temperature interval, and the midpoint of the transition is slightly higher ( $\sim 37 \text{ }^\circ\text{C}$ ).

## AmI, AmIII, and particle size

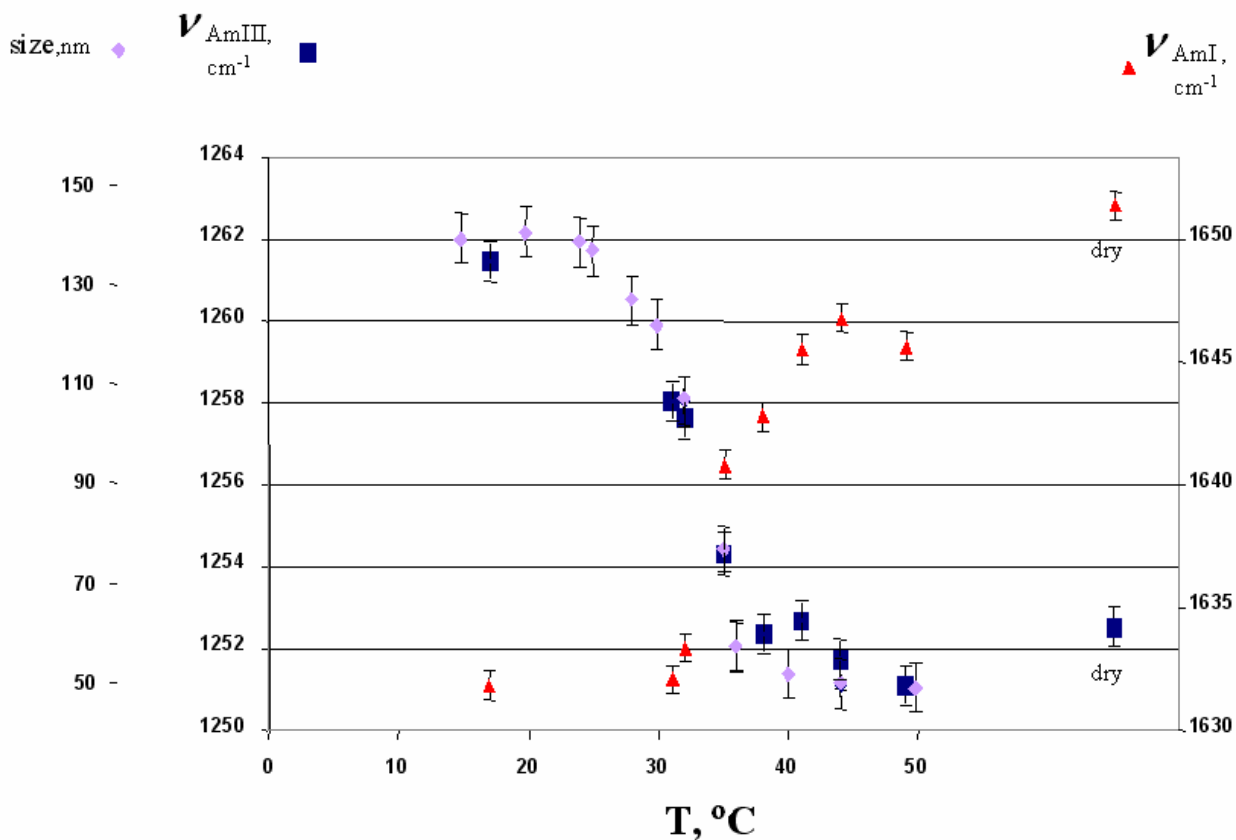


**Figure 24.** Particle size comparing to AmI and AmIII frequency.

The UVR spectra of NIPAM microgel volume phase transition support the mechanism asserting that dehydration is a major event in the transition process. We also conclude that the peptide bond remains in its *trans*- configuration regardless of the hydration state, and that different functional groups of the polymer dehydrate with different pattern.

### 3.3.2 Visible Raman. C-H stretching region

Although amide groups exhibit the highest propensity to hydrogen bonding, other parts of the polymer chain are also exposed to an aqueous environment, and therefore experience changes that can be detected spectroscopically. Isopropyl group is expected to be in different environments before and after the transition. It has been shown<sup>83,85</sup> that asymmetric C-H stretching vibration of the methyl group is sensitive to the environment. Therefore, changes occurring in that spectral region may bring additional insight on the nature of the process.

NIPAM particles contain several fragments carrying C-H bonds: methyl group ( $-\text{CH}_3$ ), methylene group ( $-\text{CH}_2$ ), and methine ( $-\text{CH}$ ) group (Figure 17). There are also  $-\text{CH}$  groups of a crosslink (N,N-methylene-bisacrylamide), but they comprise about 5 mol % of NIPAM unit and, therefore do not have much influence on the spectra. In general, each group may exhibit symmetric and antisymmetric vibration of C-H bonds, however, in each particular molecule they may or may not be detected.

We attempted to obtain a spectrum of NIPAM in  $2000 - 3600 \text{ cm}^{-1}$  region at 204 nm excitation, but it appeared that at this wavelength relatively weak stretching vibrations of C-H bonds are masked by much stronger overtones and combinations of amide bands. Figure 23 shows 204 nm excited spectra of NIPAM  $\text{D}_2\text{O}$  solution and isopropanol. Very intense and broad band of O-D stretch modes occurs at  $2300-2700 \text{ cm}^{-1}$ . Smaller peak at  $\sim 2950 \text{ cm}^{-1}$  corresponds to combinations and overtones of  $1300 - 1600 \text{ cm}^{-1}$  amide vibrations. At resonance excitation overtones may gain significant intensity to become more intense than non resonant enhanced fundamental C-H vibrations. This band is located at position where C-H stretching vibrations are expected and makes it impossible to resolve the bands. The spectrum of isopropanol is shown on the same figure to illustrate the overlap of its C-H stretching bands to complex peak of NIPAM.

Therefore, only excitation in the visible region where amide vibrations are not resonantly enhanced provides unperturbed signal of C-H stretching vibrations.

We measured spectra of aqueous solution of isopropanol at 488 nm excitation. Subtracting contribution of water band yields pure C-H vibrations of NIPAM sample. Figure 22 shows 488 nm excited spectra of isopropanol, NIPAM and NIPAM-d<sub>7</sub> in the C-H stretching region. NIPAM spectrum is very similar to that of isopropanol. The same four bands appear at roughly the same frequencies, with somewhat different relative intensities. Since NIPAM possesses a structural motif similar to isopropanol and exhibits similar spectrum, we assume the same band assignment. NIPAM-d<sub>7</sub> contains C-H groups in the main chain only, and its spectrum is free from any bands in the region 2950 – 3000 cm<sup>-1</sup>, meaning that the band of NIPAM derives entirely from isopropyl groups. The 2980 cm<sup>-1</sup> band is assigned to antisymmetric stretching vibrations of methyl groups.<sup>128-131</sup> In isopropanol the band of similar normal mode composition appears at 2970 cm<sup>-1</sup>. The presence of water upshifts this band, as shown in figure 25. In 25 % vol of isopropanol solution the band is at ~2987 cm<sup>-1</sup>. This result is consistent with the literature data.<sup>132</sup>

The environmental dependence of the C-H stretching frequency is known for many compounds. For decades, there have been debates in scientific community on whether to consider interactions of C-H groups with proton acceptors as hydrogen bonding. Opponents refer to low electronegativity of carbon which is responsible for insufficient partial charge on hydrogen atom. As a result, these low strength interactions are often masked by the multitude of other effects. Thus, many researchers believe in inability of the C-H group to form a hydrogen bond. Pimentel and McClellan,<sup>133</sup> however, note that for many compounds interactions of C-H group with proton acceptors have most of attributes of a “conventional” hydrogen bonding, such

as changes in frequency, intensity and bandwidth of the C-H stretching mode, proton chemical shift, as well as other, non spectroscopic, indications of association. The hydrogen bonding involving C-H group is not as strong as for O-H or N-H groups, and it manifests itself only with rather strong proton acceptors. In those favorable situations, however, frequency shift of C-H stretching vibration can be quite pronounced,<sup>134</sup> unambiguously indicating the presence of hydrogen bond. Complications started to arise when shifts to higher frequencies were observed.<sup>135-137</sup> Further analyses showed that other signatures of this interaction were different as well. Instead of C-H bond elongation and vibrational frequency downshift upon hydrogen bond formation, the C-H bond contracts and its stretching frequency increases. The concept of so called “anti-hydrogen bonding” or “blue shifting hydrogen bonds” appeared.<sup>138,139</sup> Several groups have been working on rationalization of this phenomenon.<sup>135,138,140-146</sup> The models include the effect of the electric field of a proton acceptor, redistributions of electron density in the proton donor molecule, and influence of the dielectric media. The concept of C-H frequency upshift upon hydration is now becoming accepted in community studying NIPAM.<sup>79,83,85,103</sup>

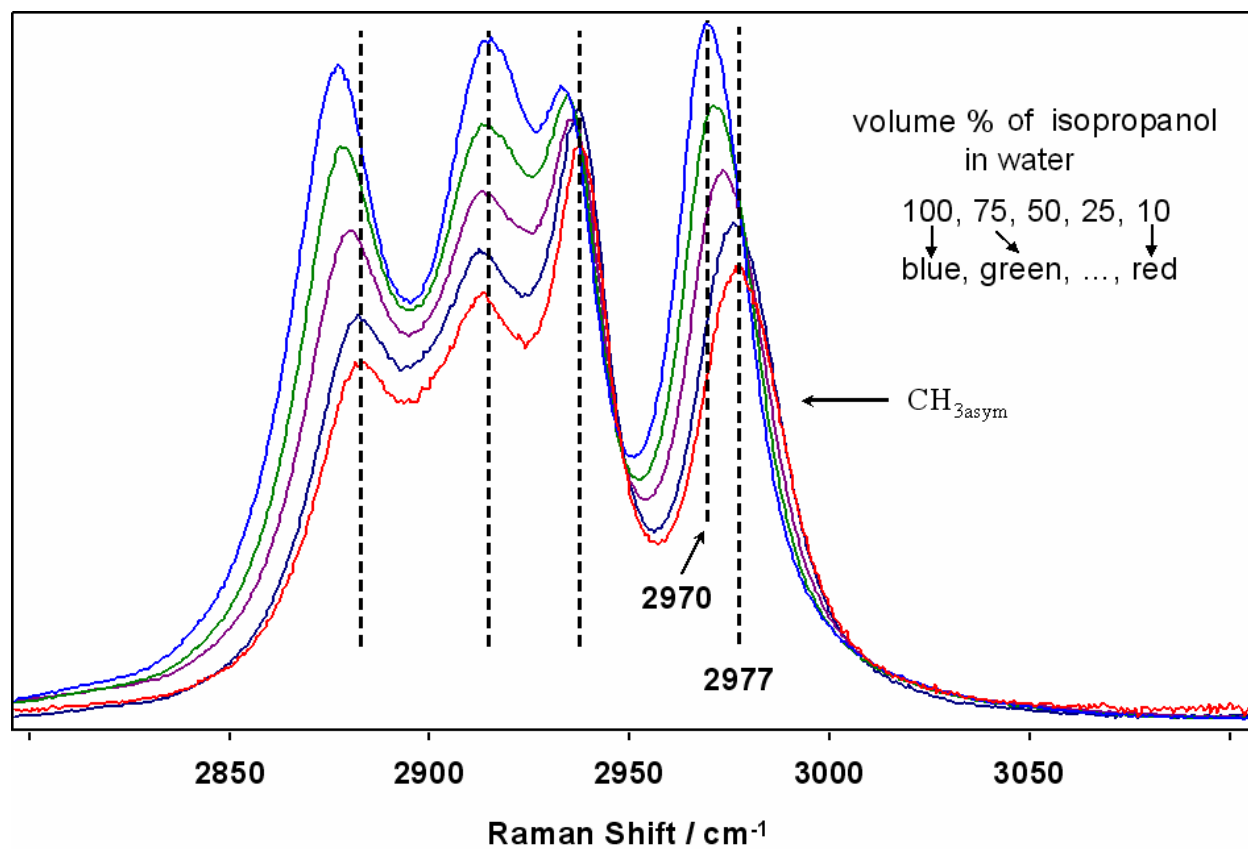


**Figure 25.** C-H stretching vibrations of iPrOH in its aqueous solutions. 488 nm excitation

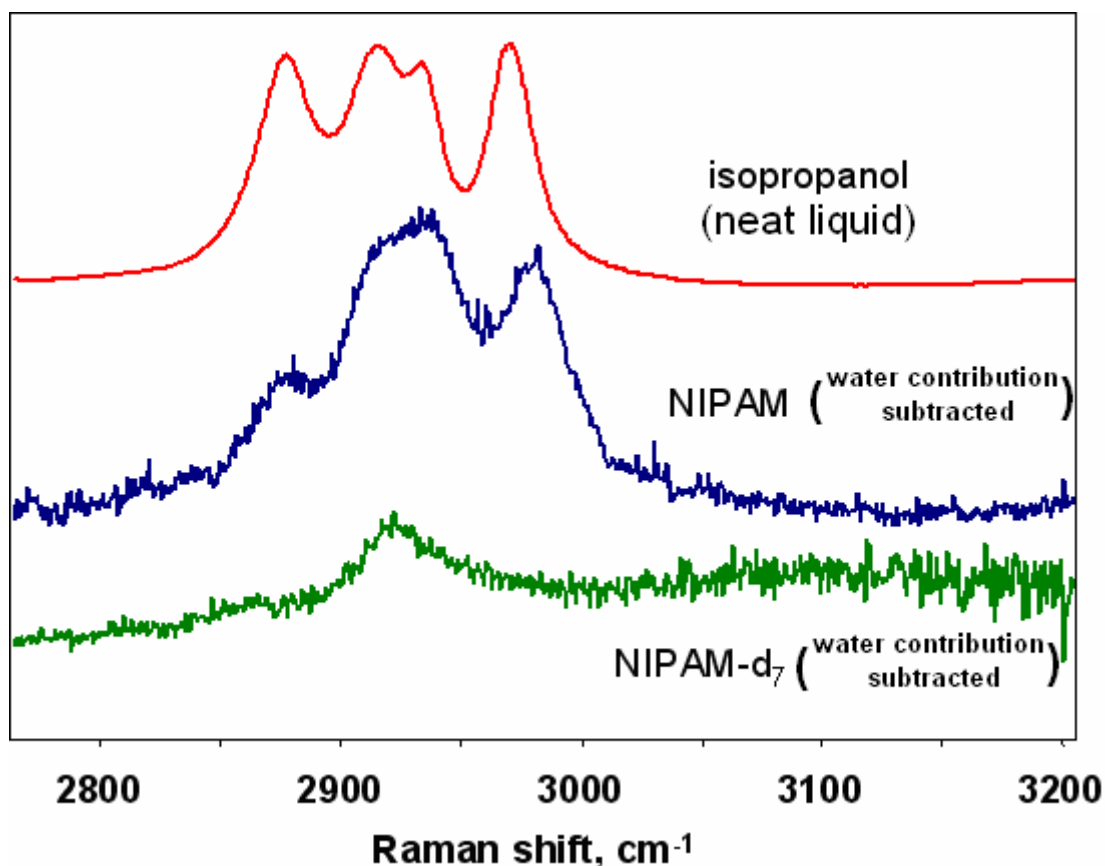


**Figure 26.** 488 nm excited Raman spectra of PNIPAM and PNIPAM-d<sub>7</sub> in comparison to isopropanol.

To aid the band assignment of NIPAM C-H stretching vibrations we compare its spectra to that of isopropanol, since they both possess a similar structural unit (isopropyl group). The spectrum of isopropanol has four distinct bands in the C-H stretching region (Figures 25, 26). Although there are discrepancies in assigning low frequency bands, the highest frequency band is unambiguously assigned to an asymmetric C-H vibration of methyl groups.<sup>128-131</sup>

The effect of hydration on hydrophobic group vibrations is being discussed in the literature.<sup>83,139,140,142,147</sup> Although the nature of this effect still remains controversial, the peak position can be used to monitor solvent exposure of the methyl group.

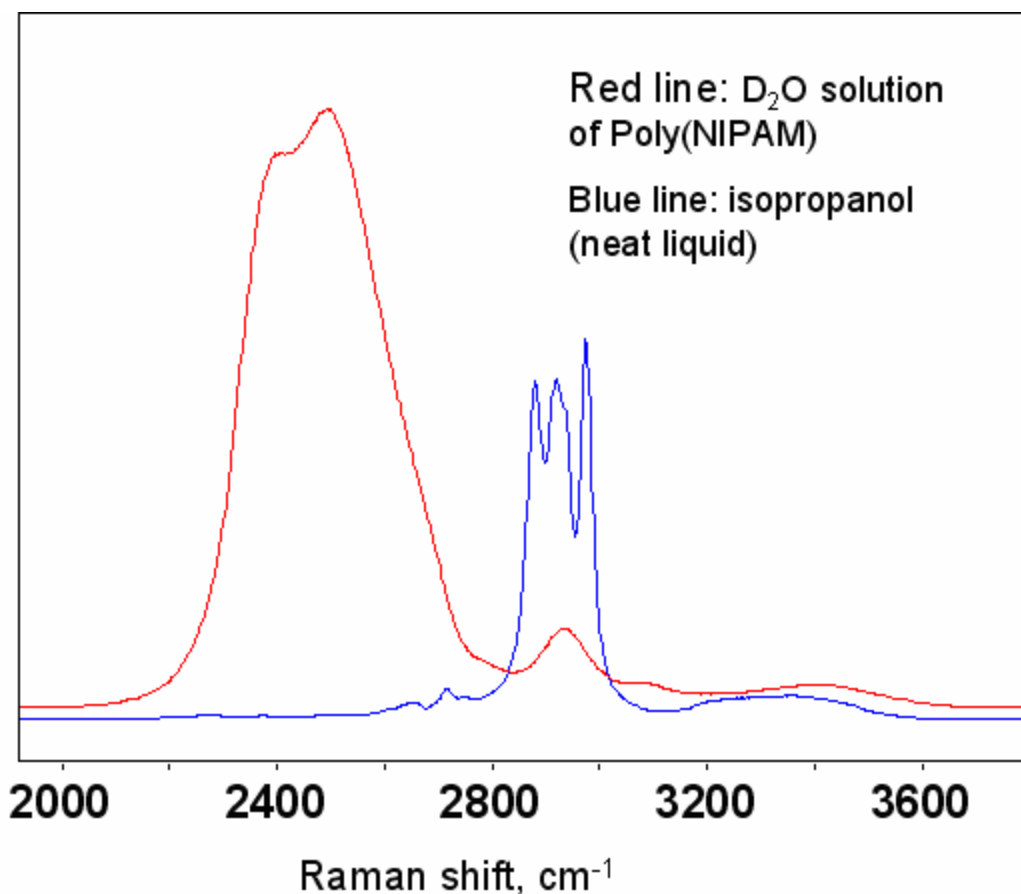


**Figure 27.** 204 nm excited spectra of isopropanol and PNIPAM D<sub>2</sub>O solution.

Figure 28 shows 488 nm excited Raman spectra of NIPAM aqueous solutions at temperatures from 5 to 45 °C where contribution from water was subtracted. At temperatures 30 °C and below the band position remains at ~2980 cm<sup>-1</sup>, while at higher temperatures it gradually shifts to 2975 cm<sup>-1</sup>. Most of that change occurs in a narrow temperature interval 30-40 °C, while outside of that range the shift is negligible. Figure 29 demonstrates the peak position with respect to temperature. The characteristic S-shape curve indicates that the observing change correlates with the phase transition. According to the Figure 29 curve the transition temperature is around 35 °C, which is close to that determined by turbidity.

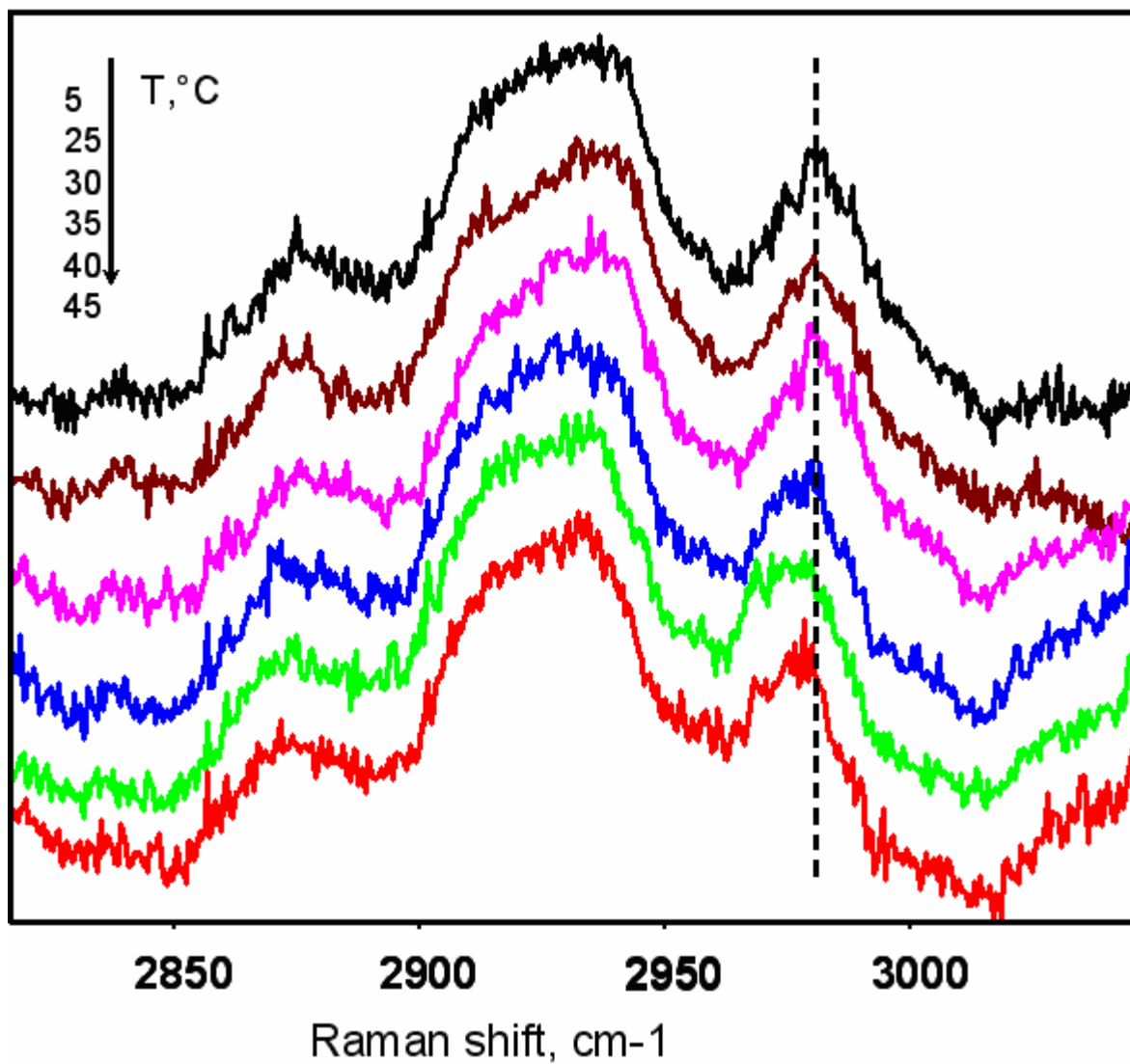
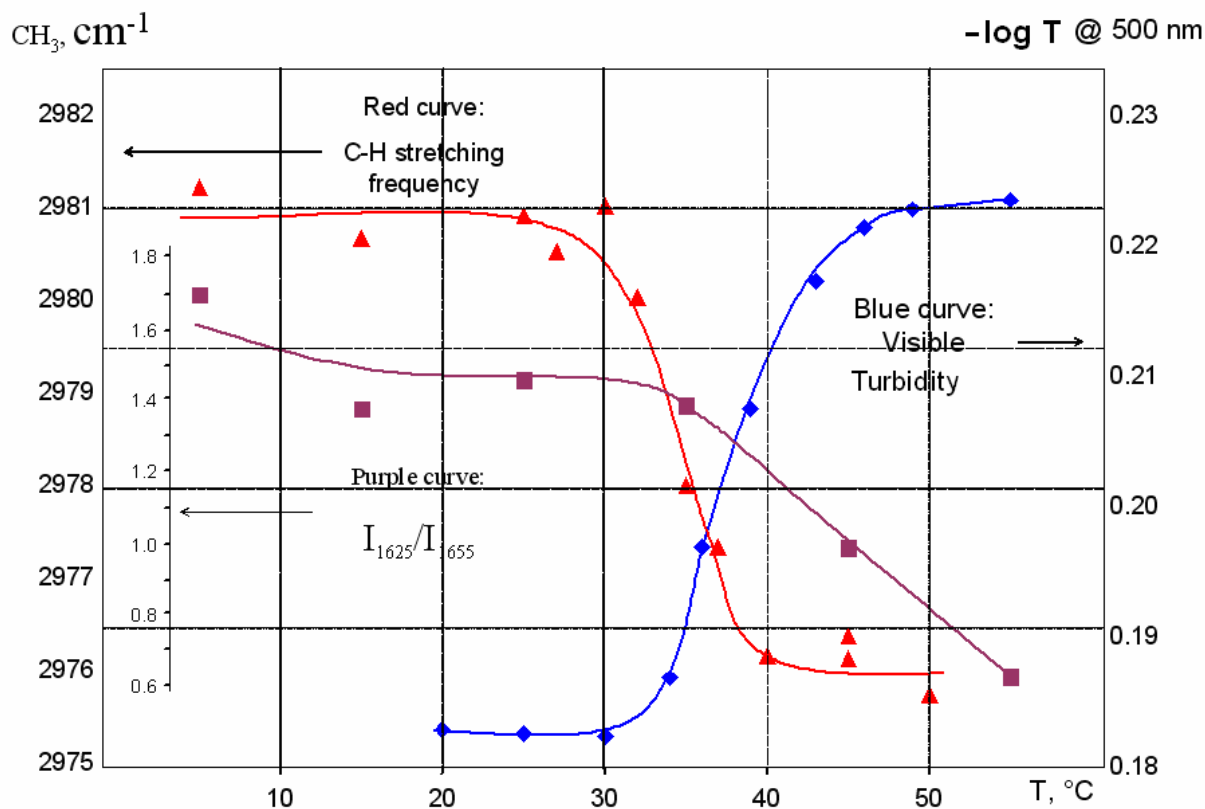


Figure 28. 488 nm excited Raman spectra of PNIPAM at indicated temperatures.



**Figure 29.** Comparison of different spectroscopic markers of PNIPAM transition: Position of C-H stretching peak; Turbidity of the solution; Ratio of Amide I peaks.

Qualitatively the C-H stretching frequency shift follows the Amide band trends. The largest frequency change occurs around 35 °C, which corresponds to dehydration. Then dehydration is followed by reorganization of chains in a search for favorable contacts. The change is less than that of Amide bands, which is expected, since C-H groups are usually less sensitive to hydration than C=O or N-H groups are. Unlike the amide bands, C-H vibrations do not report on any specific interactions, since they are sensitive to overall environmental changes which in the case of the volume phase transition consist of dehydration of the particles.

### 3.3.3 Kinetics of the phase transition

In order to obtain information on kinetics of the phase transition we performed a laser induced temperature jump experiment. The UV Raman spectra were recorded at the following delay times after the heating pulse: 20 ns, 50 ns, 80 ns, 100 ns, 200 ns, 400 ns, 500 ns, 700 ns, 900 ns, 1.2  $\mu$ s, 2  $\mu$ s, 3  $\mu$ s, 4  $\mu$ s, 9  $\mu$ s, 11  $\mu$ s, 17  $\mu$ s, 25  $\mu$ s, 80  $\mu$ s, and 100  $\mu$ s. Figure 30 shows the spectra obtained at selected delay times.

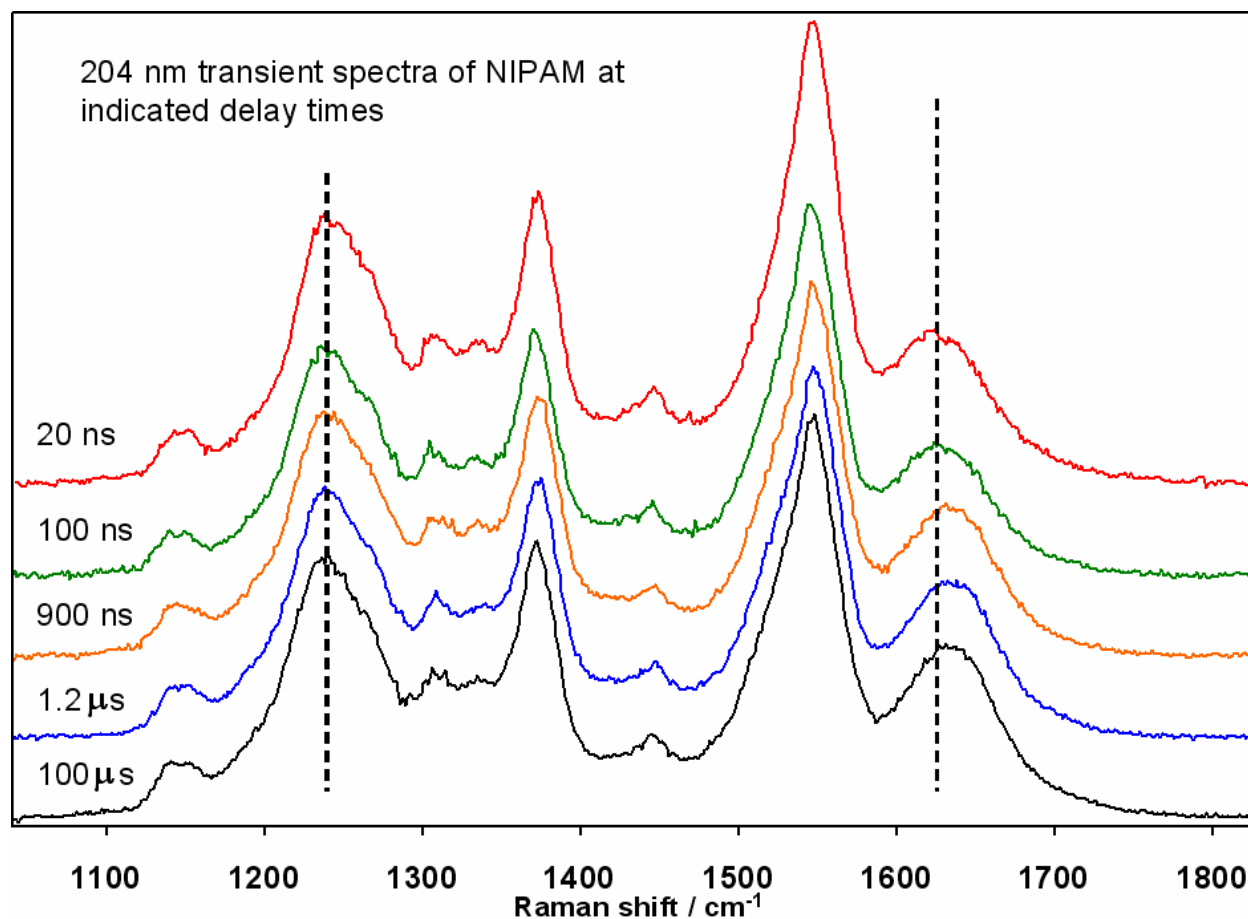


Figure 30. 204 nm transient spectra of NIPAM at selected delay times.

It can be seen that spectra at longer delay times are similar to steady state spectra at high temperatures, (Figure 18) while spectra at shorter times after T-jump differ little from initial sample, not perturbed by a heat pulse. We modeled transient spectra with a set of Gaussian and Lorentzian bands, as shown in Figure 31. In contrast to steady state spectra modeling, we limit areas under AmI and AmIII bands to single peaks. This is necessary in order to avoid larger errors in peak position when modeling of the band is achieved with two or more peaks.

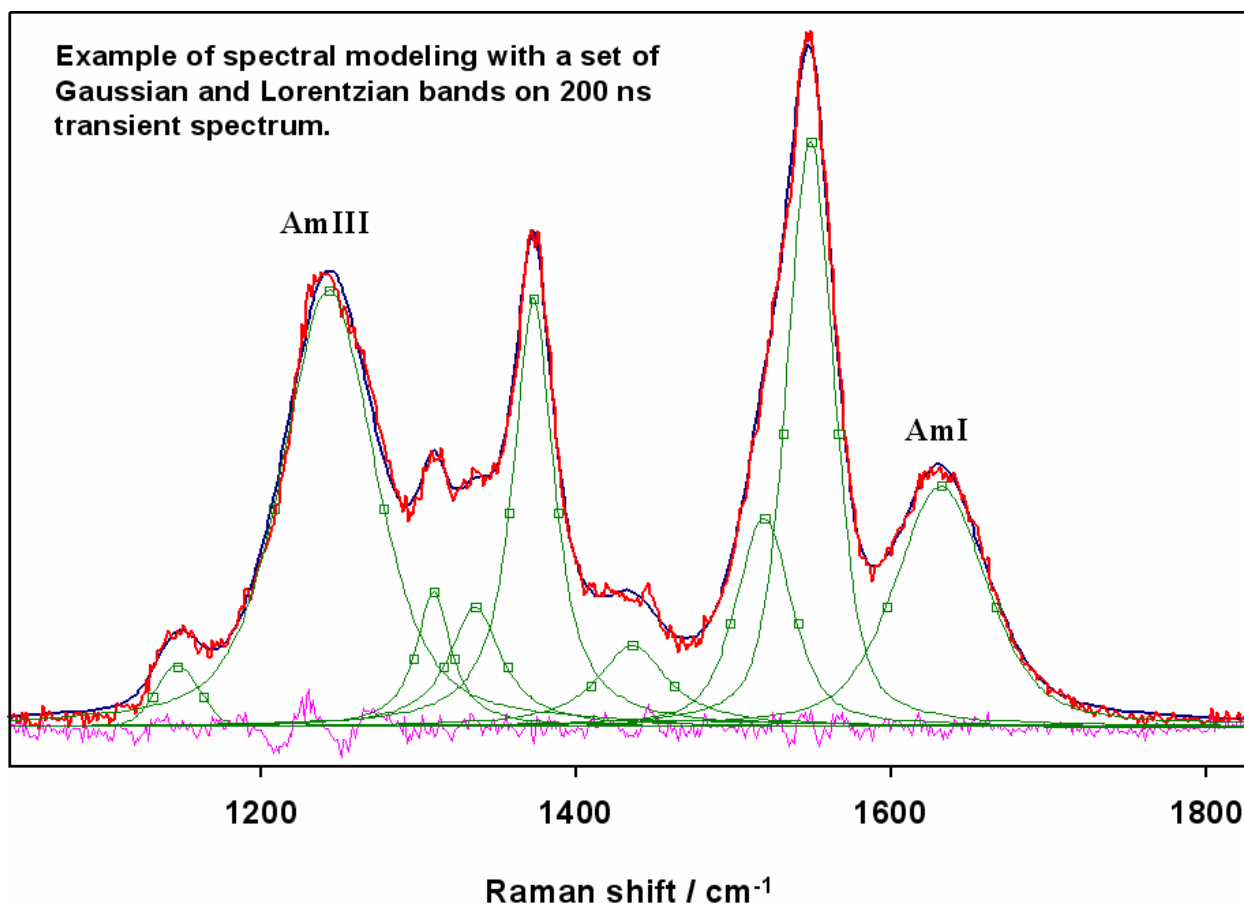


Figure 31. An example of transient spectra modeling.

In order to detect small changes reliably, we subtracted corresponding spectra at initial temperature from each transient spectrum. These difference spectra show changes that occur in a

time period between heating pulse and corresponding delay time. Figure 32 shows such spectra at selected delay times. Sinusoidal feature in a difference spectrum, as the one shown for AmIII peak in 50 ns spectrum, corresponds to a frequency shift in subtracted spectrum with respect to the original spectrum. When such sinusoidal shape is symmetric, as in 50 ns, 2  $\mu$ s and 25  $\mu$ s, it corresponds to a peak shift with constant intensity. In some cases, however, peak and trough of that sinusoid are different with the extreme that only peak remains, as in 20 ns and 100  $\mu$ s spectra, such difference spectra indicate that both peak frequency and intensity change. The AmI band is always a peak in difference spectra. That is expected, since steady state spectra demonstrate significant intensity increase of the AmI band in high temperature spectra.

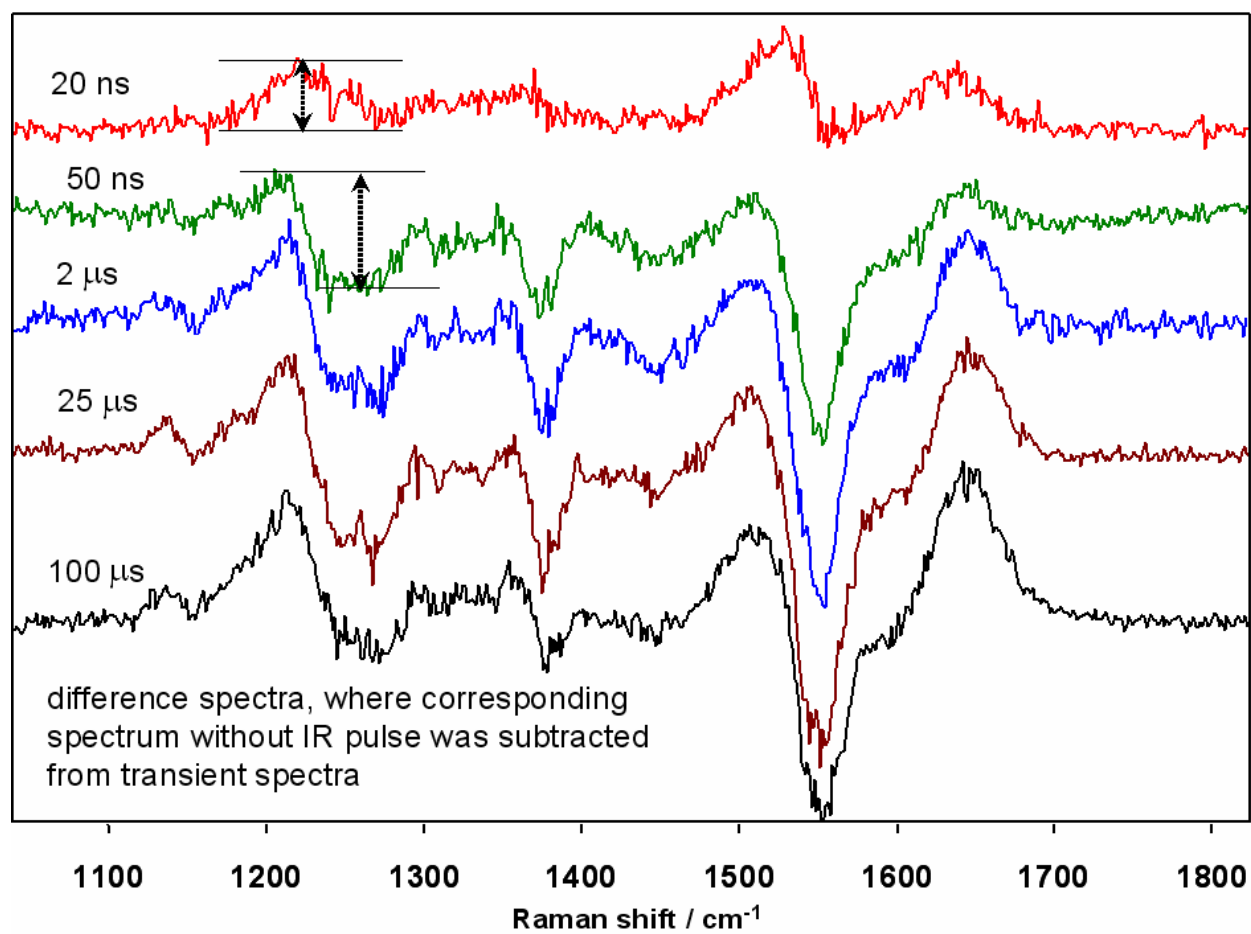
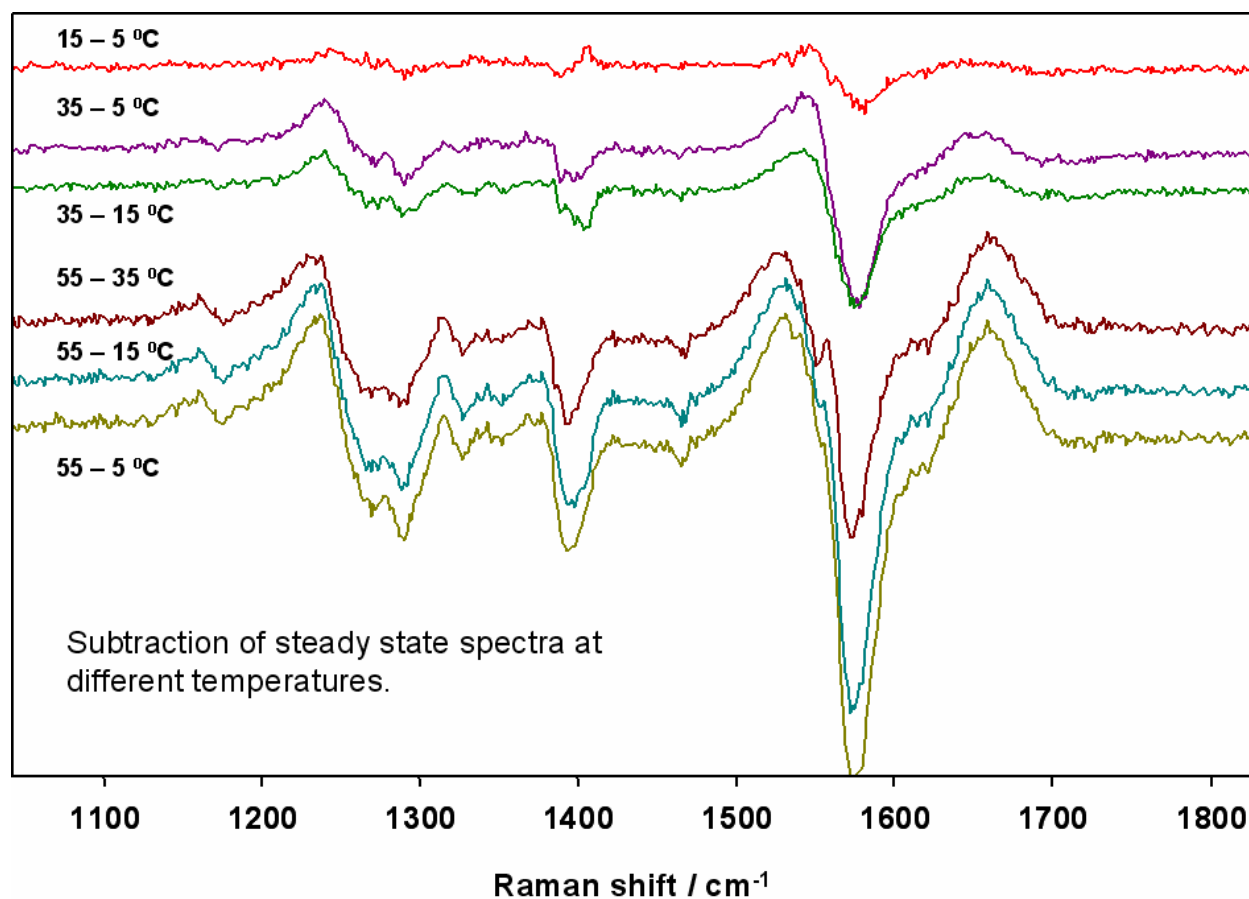


Figure 32. Difference spectra hot-cold at indicated delay times.



**Figure 33.** Difference spectra obtained by subtraction of steady state spectra at indicated temperatures.

These transient difference spectra are similar to steady state difference spectra shown in Figure 33. Subtracting a 5 °C spectrum from that at 15 °C yields a difference spectrum much like the transient one at 20 ns delay time. The temperature interval 5 – 15 °C is far from the transition temperature of ~35 °C, which means that both 5 and 15 °C spectra correspond to NIPAM in a swollen state. The difference between 5 and 15 °C spectra of NIPAM is not due to its different conformations, but rather due to different hydrogen bonding strength of amides to water at different temperatures, similar to phenomenon observed in extended conformations of peptides.<sup>35,36,66</sup> These band shifts in peptide spectra were attributed to gradual weakening of hydrogen bonding strength between amides of peptide bond and water. Similar mechanism

should exist here as well. The similarity of 15 – 5 °C steady state difference spectrum to 20 ns transient spectrum indicates that polymer backbone remains in the same conformation for at least 20 ns after heating pulse. Only after 50 ns we start to observe spectral changes attributable to transformations in NIPAM conformation.

Larger changes are observed in difference spectra of 35 – 5 °C and 35 -15 °C, since 35 °C is in the middle of the transition process. Even larger changes appear on 55 – 35 °C, 55 – 15 °C, and 55 – 5 °C difference spectra, with increased intensity of the AmI band and difference feature of the AmIII band. These differences become bigger as difference in temperature of subtracting spectra increases. These changes are qualitatively similar to those observed in transient difference spectra as delay time after heating pulse increases.

To quantitate changes occurring with both AmIII and AmI bands we monitored changes in intensity of AmIII and AmI peaks (or total difference from peak to trough as it is shown in Figure 32) in difference spectra. Figure 34 shows time dependence of the AmIII and the AmI band intensity. The surprising finding is that intensity has logarithmic dependence on time (a straight line in  $I-\ln(\text{time})$  coordinates). The lines represent the best fit to data points with the restriction that slopes of both AmI and AmIII lines were set to be the same. All three lines are of the same general type:

$$I = A \cdot \ln(t) + B \tag{1}$$

where  $I$  – intensity of the peak (or peak to trough difference),  $t$  – time,  $A$  and  $B$  – coefficients. The following parameters were obtained for each curve:

$$\text{AmIII: } A = 5.0029, B = 43.562, R^2 = 0.914;$$

$$\text{AmI short delay times: } A = 5.0666, B = 33.924, R^2 = 0.7928;$$

$$\text{AmI long delay times: } A = 5.0465, B = 22.463, R^2 = 0.9402.$$

A statistical parameter  $R^2$  describes how well the theoretical curve represents experimental data. For two out of three curves, the values of  $R^2$  are greater than 0.90 which is typically considered acceptable. A smaller value of  $R^2$  for AmI at short delay times is in part due to a drop in both AmIII and AmI values at 700 ns, which is likely due to experimental variation. It produces greater impact on AmI line at short delay times, than on AmIII line, which has more data points, thus the influence of a single point is less.

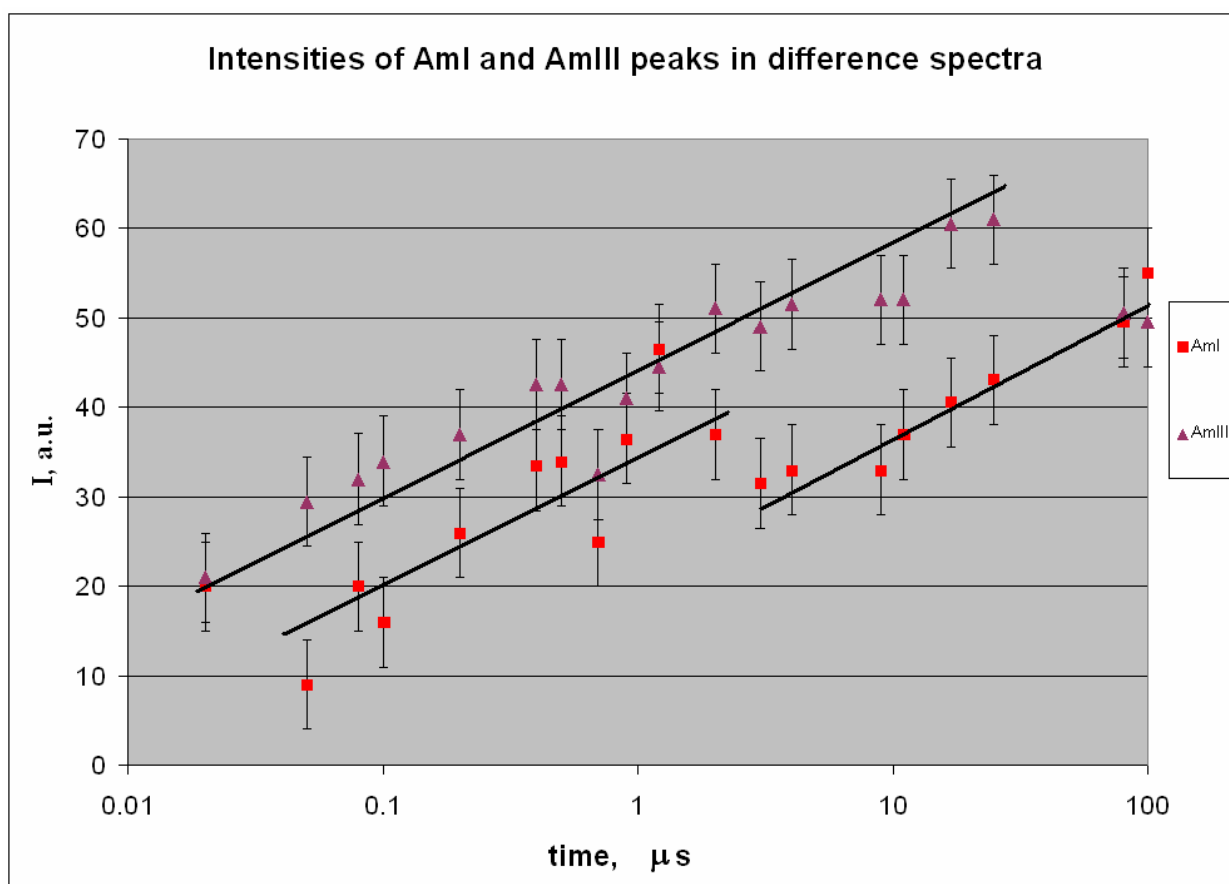


**Figure 34.** Time dependence of AmI and AmIII intensities in difference spectra.

The peak to trough intensity in difference spectra experimentally correlates with the peak frequency in original hot spectra, which in turn is related to the environment of the

corresponding group, (N-H for AmIII, and C=O for AmI) and describes dehydration of the NIPAM during transition. Such logarithmic kinetics of dehydration in polymers was not observed previously.<sup>116,148-150</sup> The observed kinetics indicates that the process is not a simple equilibrium between two states, and has more complex physics.

Similar logarithmic kinetics is known for polymers undergoing a glass transition.<sup>151-154</sup> That is a transition between two states with greatly different mobility of molecules. A motion of a polymer chain surrounded by other chains depends on the amount of free volume which can be occupied as a result of movement. According to Williams-Landel-Ferry<sup>155</sup> probability of molecular motion is expressed as

$$P = \exp\left(\frac{-B}{f}\right) \quad (2)$$

where  $P$  is probability of change in chain conformation,  $B$  is coefficient and  $f$  is fractional free volume. Probability of the event increases over time, and when the quantity  $tP$  (where  $t$  is time) achieves a certain value, a conformational change may take place. Multiplying the equation (2) by  $t$  and taking log from each side yields:

$$\log tP = -B/f + \log t \quad (3)$$

and after differentiating:

$$\Delta \log t = B\Delta(1/f) \quad (4)$$

where  $t$  is time after perturbation of the polymer.

For most polymers their mechanical properties such as relaxation and creep moduli are proportional to free volume and therefore to logarithm of time after onset of the transition.<sup>152,154</sup>

Such similarity of NIPAM transition kinetics to that of a polymer glass transition suggests that the NIPAM volume phase transition is similar to glass transition of polymers. The NIPAM transition involves significant rearrangement of polymer chains from extended

conformations in a large swollen particle to folded conformations in a dehydrated compact particle as shown in Figure 13. Motion of a chain in a particle is hindered by other chains which are cross linked to it. As particles begin to shrink, mechanical strain is imposed on chains and they behave similar to polymer chains undergoing glass transition. Therefore, we conclude that kinetics of particles' collapse is limited by relaxation of strain imposed on polymer chains. Different behavior of the AmIII band after 80  $\mu$ s and slight change in the AmI band intensity after 2  $\mu$ s may indicate additional processes begin to play a role at longer time scale. Further investigations are needed in order to clarify the mechanism.

### 3.4 CONCLUSIONS

We synthesized hydrogel colloidal particles of PNIPAM and PNIPAM-d<sub>7</sub>. We applied UV Raman and normal Raman spectroscopies to study PNIPAM volume phase transition. To the best of our knowledge this is the first example of use of UV Raman in PNIPAM studies. We have shown, that our methods support findings of other researchers who used other techniques: IR, NMR, fluorescent spectroscopies, and others. Comparing the spectra of PNIPAM to that of PNIPAM-d<sub>7</sub> we were able to make an assignment of spectral bands. Our results confirm that PNIPAM transition involves dehydration of both hydrophobic and hydrophilic moieties of the polymer structure. In addition, we found that the peptide group of the polymer exists in a *trans*-configuration in both states, before and after the transition, in contrast to some suggestions.<sup>105</sup> We also showed that in the first 25  $\mu$ s of the transition peak positions of AmI and AmIII bands change with logarithm of time after temperature jump. This suggests that in this time scale the

kinetics of the NIPAM volume phase transition is limited by relaxation of strain in the polymer chains.

### 3.5 FUTURE WORK

The following questions on NIPAM volume phase transition need to be addressed. First, further band assignment in the amide region is needed in order to have greater insight on the phenomenon. In particular, the AmIII band definitely contains several peaks, which may bring additional information on the conformation. That could be achieved by higher resolution detection system.

Second, better signal to noise spectra and several replicate measurements of transient spectra are needed to determine kinetics more reliably and relate this information to theoretical models of the phase transition. Experiments with more stable T-jump values over broader range of temperatures are necessary. Spectra free from oxygen interference in the AmII region would make another band available for kinetic studies.

Extending T-jump methodology to visible region would allow obtaining kinetics of the isopropyl group dehydration. This information is extremely valuable in order to solve a long existed controversy on whether hydrophilic or hydrophobic part of the polymer initiates dehydrates. Knowledge of dehydration kinetics of isopropyl group would allow to significantly improve understanding of the NIPAM phase transition. That would also have implications for protein folding science.

#### 4.0 DEVELOPMENT OF NEW MARKERS OF PEPTIDE CONFORMATIONS. C<sub>α</sub>-H STRETCHING.

Over the past few years our group have developed the methodology for correlating the observed AmIII<sub>3</sub> band position with the backbone Ψ dihedral angle and hydrogen bonding state of the peptide bond. Current efforts are aimed at refining this relationship to account for the impact of Φ dihedral angle on the observed AmIII<sub>3</sub> band position. Simultaneously, we are examining the peptide Raman spectra for vibrations that can provide complimentary information that can further enhance our understanding of protein folding.

Recent *ab initio* calculations by Mirkin and Krimm<sup>156</sup> suggested a conformation and hydration sensitivity for the C<sub>α</sub>-H, stretching band frequency. The C<sub>α</sub>-D isotope is found to be particularly sensitive to conformation and hydration effects. The C<sub>α</sub>-H stretching band is located in the 2800-3000 cm<sup>-1</sup> spectral region has been largely ignored by protein spectroscopists, since it was believed that the spectral region was dominated by local, uncoupled vibrations and hence was believed to be independent of conformation and environment change. However, Mirkin and Krimm demonstrated that for dialanine peptide the C<sub>α</sub>-H is not a 100 % localized mode. The diagonal stretch force constant ( $f(C_{\alpha}\text{-H})$ ) and off-diagonal force constants ( $f(C_{\alpha}\text{-H}, \text{NC}_{\alpha}\text{C}), f(C_{\alpha}\text{-H}, \text{NC}_{\alpha}\text{-H})$ ) vary with local Φ, Ψ angles; furthermore, nearest-neighbor hydrogen bonded water structure is impacted by local conformation, differential hydrogen bonding patterns by two nearest peptides group are expected to impact the C<sub>α</sub>-H stretching frequency.

Our initial work indicated that the non-resonance enhanced  $C_{\alpha}$ -H(D) band intensity is negatively impacted by high self-absorption in the UV; furthermore, the overtones of amide bands interfere with the  $C_{\alpha}$ -H(D) stretching band. In order to rectify these problems, we have recently constructed a visible Raman spectrometer that can operate at 488-532 nm. Our preliminary results appear to support Mirkin and Kirmm's proposal. At 488 nm excitation we examined anhydrous (solid) and hydrated (liquid solution) forms of acetyl-alanine. Upon transference from solid to liquid phase the  $C_{\alpha}$ -H stretching band up shifts from 2865 to 2885  $\text{cm}^{-1}$ . The observed shift likely contains contributions from both hydration and conformation changes. We should note that in case of acetylalanine the C-H stretching vibrations of methyl side chains contribute in the same region as well, however, as shown in Figure 35 the  $C_{\alpha}$ -H and methyl C-H stretching bands are well resolved. We propose a study of alanine based  $\alpha$ -helical peptide (AP) to examine the impact of defined conformation changes on  $C_{\alpha}$ -H(D) stretching frequency.

This study can potentially revolutionize our understanding of protein folding. Changes in  $C_{\alpha}$ -H(D) band position can provide complimentary information to augment the conformation sensitive results extracted from the  $\text{AmIII}_3$  band position. In a large proteins with  $C_{\alpha}$ -D substitutions we can potentially track both local ( $C_{\alpha}$ -D<sub>s</sub>) and global ( $\text{AmIII}_3$  band contributions of all non-substituted peptide bonds) conformation changes in the Ramachandran space. Furthermore, the methodology developed for correlating  $C_{\alpha}$ -H(D) frequency position with backbone conformation will allow Raman and IR spectroscopists to measure protein folding/unfolding in the Ramachandran space, albeit on a more limited basis than afforded by UVRS. Thus this work has potential to revolutionize the study of protein folding for spectroscopists in general.

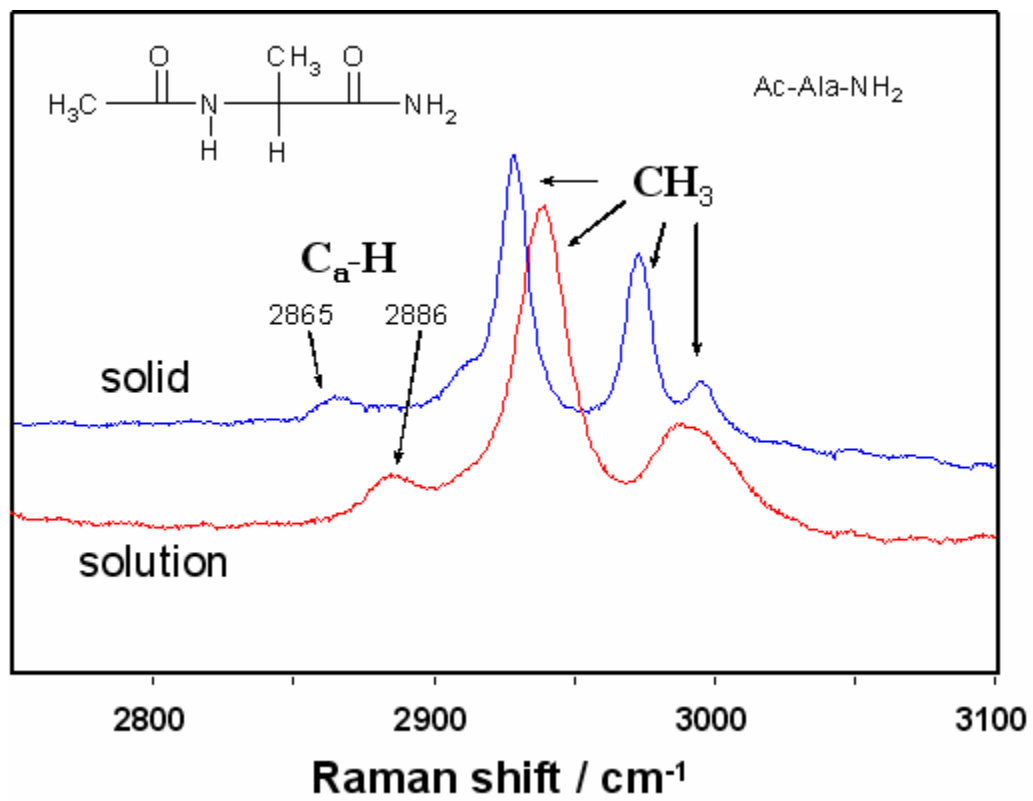


**Figure 35.** 488 nm excited Raman spectra of Ac-Ala-NH<sub>2</sub> in the solid state and solution at a concentration of 10 mg/ml.

## BIBLIOGRAPHY

- (1) Creighton, T. E. *Proteins: Structures and Molecular Properties*; 2nd ed.; W.H. Freeman: New York, 1993.
- (2) Anfinsen, C. B. *Science (Washington, DC, United States)* **1973**, *181*, 223-230.
- (3) Levinthal, C. *Extr. J.Chim. Phys.* **1968**, *65*, 44-45.
- (4) Ramachandran, G. N. *Struct. Chem. Mol. Biol.* **1968**, 77-87.
- (5) Ramachandran, G. N.; Sasisekharan, V. *Advances in Protein Chemistry* **1968**, *23*, 283-438.
- (6) Dill, K. A. *Biochemistry* **1990**, *29*, 7133-7155.
- (7) Garrett, R. G., Grisham, C. M. *Biochemistry*; 2nd ed.; Saunders College Publishing: Philadelphia, 1999.
- (8) Pain, R. H. *Mechanisms of Protein Folding*; Oxford University Press: New York, 1994.
- (9) Baker, E. N.; Hubbard, R. E. *Prog. Biophys. Mol. Biol.* **1984**, *44*, 97-179.
- (10) McColl, I. H.; Blanch, E. W.; Hecht, L.; Barron, L. D. *J. Am. Chem. Soc.* **2004**, *126*, 8181-8188.
- (11) Tanford, C. *The Hydrophobic Effect: Formation of Micelles and Biological Membranes. 2nd Ed*; Wiley: New York, 1980.
- (12) Blokzijl, W.; Engberts, J. B. F. N. *Angew. Chem. Int. Ed. Engl.* **1993**, *32*, 1545-1579.
- (13) Holmes, K. C.; Blow, D. M. *The Use of X-ray Diffraction in the Study of Protein and Nucleic Acid Structure*, 1966.
- (14) Clore, G. M.; Gronenborn, A. M. *Nature Structural Biology* **1997**, *4*, 849-853.
- (15) Clore, G. M.; Gronenborn, A. M. *Trends in Biotechnology* **1998**, *16*, 22-34.
- (16) Kulikov, A. V.; Likhtenshtein, G. I.; Rozantsev, E. G.; Suskina, V. I.; Shapiro, A. B. *Biofizika* **1972**, *17*, 42-48.
- (17) Chirgadze, Y. N. *Infrared Spectra and Structure of Polypeptides and Proteins*, 1965.
- (18) Jas, G. S.; Eaton, W. A.; Hofrichter, J. *Journal of Physical Chemistry B* **2001**, *105*, 261-272.
- (19) Manas, E. S.; Getahun, Z.; Wright, W. W.; DeGrado, W. F.; Vanderkooi, J. M. *J. Am. Chem. Soc.* **2000**, *122*, 9883-9890.
- (20) Allan, V. J. *Protein Localization by Fluorescence Microscopy: A Practical Approach*; Oxford Univ Press: Oxford, 2000.
- (21) Hof, M.; Hutterer, R.; Fidler, V. *Fluorescence Spectroscopy in Biology: Advances Methods and Their Applications to Membranes, Proteins, DNA, and Cells*; Springer: Berlin, 2005.

- (22) Khamidov, D. K.; Saatov, T. S.; Khakimov, P. A. *Ultraviolet Fluorescence of Proteins and Cells*; Fan: Tashkent, 1982.
- (23) Nairn, R. *Fluorescent Protein Tracing. 4th Ed*; Churchill Livingstone: New York, 1976.
- (24) Woody, R. W. *Circular Dichroism and the Conformational Analysis of Biomolecules* **1996**, 25-67.
- (25) Fasman, G. D. *Circular Dichroism and the Conformational Analysis of Biomolecules*, 1996.
- (26) Ozdemir, A.; Lednev, I. K.; Asher, S. A. *Biochemistry* **2002**, *41*, 1893-1896.
- (27) Barron, L. D.; Hecht, L.; Ford, S. J.; Bell, A. F.; Wilson, G. *Journal of Molecular Structure* **1995**, *349*, 397-400.
- (28) McColl, I. H.; Blanch, E. W.; Hecht, L.; Kallenbach, N. R.; Barron, L. D. *J. Am. Chem. Soc.* **2004**, *126*, 5076-5077.
- (29) Zhu, F.; Isaacs, N. W.; Hecht, L.; Barron, L. D. *Structure (Cambridge, MA, United States)* **2005**, *13*, 1409-1419.
- (30) Spiro, T. G. *Biological Applications of Raman Spectroscopy, Vol. 1: Raman Spectra and the Conformations of Biological Macromolecules*, 1987.
- (31) Thomas, G. J., Jr. *Biopolymers* **2002**, *61*, 214-225.
- (32) Asher, S. A. *Analytical Chemistry* **1993**, *65*, 59A-66A.
- (33) Asher, S. A. *Analytical Chemistry* **1993**, *65*, 201A-210A.
- (34) Chi, Z.; Asher, S. A. *Journal of Physical Chemistry B* **1998**, *102*, 9595-9602.
- (35) Asher, S. A.; Mikhonin, A. V.; Bykov, S. V. *J. Am. Chem. Soc.* **2004**, *126*, 8433-8440.
- (36) Lednev, I. K.; Karnoup, A. S.; Sparrow, M. C.; Asher, S. A. *J. Am. Chem. Soc.* **1999**, *121*, 8074-8086.
- (37) Spiro, T. G. *Biological Applications of Raman Spectroscopy, Vol. 3: Resonance Raman Spectra of Heme and Metalloproteins*, 1988.
- (38) Cleland, J. L. *Protein Folding: In Vivo and In Vitro, Developed from a Symposium held at the 203rd National Meeting of the American Chemical Society in San Francisco, Calif. April 5-10, 1992. [In: ACS Symp. Ser., 1993; 526]*, 1993.
- (39) Yang, J. T. *Chemtracts: Biochemistry and Molecular Biology* **1991**, *2*, 239-244.
- (40) Alfimova, E. Y.; Likhtenshtein, G. I. *Itogi Nauki i Tekhniki, Seriya: Molekulyarnaya Biologiya* **1976**, *8*, 127-179.
- (41) Finazzi-Agro, A.; Avigliano, L. *Life Chemistry Reports* **1984**, *2*, 97-139.
- (42) Banerjee, R.; Basu, G. *FEBS Letters* **2002**, *523*, 152-156.
- (43) Gruebele, M. *Annu. Rev. Phys. Chem.* **1999**, *50*, 485-516.
- (44) Kelly, S. M.; Price, N. C. *Current Protein and Peptide Science* **2000**, *1*, 349-384.
- (45) Mulkerrin, M. G. *Spectroscopic Methods for Determining Protein Structure in Solution* **1996**, 5-27.
- (46) Lewis, I. R.; Edwards, H. G. M. *Handbook of Raman spectroscopy. [In: Pract. Spectrosc., 2001; 28]*, 2001.
- (47) Sweeney, J. A.; Asher, S. A. *Journal of Physical Chemistry* **1990**, *94*, 4784-4791.
- (48) Matsuno, M.; Takeuchi, H. *Bulletin of the Chemical Society of Japan* **1998**, *71*, 851-857.
- (49) Chi, Z.; Chen, X. G.; Holtz, J. S. W.; Asher, S. A. *Biochemistry* **1998**, *37*, 2854-2864.

- (50) Bochicchio, B.; Tamburro, A. M. *Chirality* **2002**, *14*, 782-792.
- (51) Martino, M.; Bavoso, A.; Guantieri, V.; Coviello, A.; Tamburro, A. M. *J. Mol. Struct.* **2000**, *519*, 173-189.
- (52) Stapley, B. J.; Creamer, T. P. *Protein Sci.* **1999**, *8*, 587-595.
- (53) Mezei, M.; Fleming, P. J.; Srinivasan, R.; Rose, G. D. *Proteins: Structure, Function, and Bioinformatics* **2004**, *55*, 502-507.
- (54) Kelly, M. A.; Chellgren, B. W.; Rucker, A. L.; Troutman, J. M.; Fried, M. G.; Miller, A.-F.; Creamer, T. P. *Biochemistry* **2001**, *40*, 14376-14383.
- (55) Shi, Z.; Olson, C. A.; Rose, G. D.; Baldwin, R. L.; Kallenbach, N. R. *Proc. Natl. Acad. Sci. U.S.A.* **2002**, *99*, 9190-9195.
- (56) Mezei, M.; Fleming, P. J.; Srinivasan, R.; Rose, G. D. *Proteins* **2004**, *55*, 502-507.
- (57) Stapley, B. J.; Creamer, T. P. *Protein Science* **1999**, *8*, 587-595.
- (58) Gnanakaran, S.; Hochstrasser, R. M.; Garcia, A. E. *Proc. Natl. Acad. Sci. U.S.A.* **2004**, *101*, 9229-9234.
- (59) Thanki, N.; Thornton, J. M.; Goodfellow, J. M. *J. Mol. Biol.* **1988**, *202*, 637-657.
- (60) Walsh, S. T. R.; Cheng, R. P.; Wright, W. W.; Alonso, D. O. V.; Daggett, V.; Vanderkooi, J. M.; DeGrado, W. F. *Prot. Sci.* **2003**, *12*, 520-531.
- (61) Daggett, V.; Levitt, M. *J. Mol. Biol.* **1992**, *223*, 1121-1138.
- (62) Luo, P.; Baldwin, R. L. *Proceedings of the National Academy of Sciences of the United States of America* **1999**, *96*, 4930-4935.
- (63) Song, S.; Asher, S. A. *J. Am. Chem. Soc.* **1989**, *111*, 4295-4305.
- (64) Mikhonin, A. V.; Ahmed, Z.; Ianoul, A.; Asher, S. A. *J. Phys. Chem. B* **2004**, *108*, 19020-19028.
- (65) Elliott, A.; Malcolm, B. R. *Proc. R. Soc. (London)* **1959**, *A249*, 30-41.
- (66) Lednev, I. K.; Karnoup, A. S.; Sparrow, M. C.; Asher, S. A. *J. Am. Chem. Soc.* **2001**, *123*, 2388-2392.
- (67) Mikhonin, A. V.; Myshakina, N. S.; Bykov, S. V.; Asher, S. A. *J. Am. Chem. Soc.* **2005**, *127*, 7712-7720.
- (68) Torii, H.; Tatsumi, T.; Tasumi, M. *J. Raman Spectrosc.* **1998**, *29*, 537-546.
- (69) Huang, R.; Kubelka, J.; Barber-Armstrong, W.; Silva, R. A. G. D.; Decatur, S. M.; Keiderling, T. A. *Journal of the American Chemical Society* **2004**, *126*, 2346-2354.
- (70) Scharnagl, C.; Reif, M.; Friedrich, J. *Biochimica et Biophysica Acta, Proteins and Proteomics* **2005**, *1749*, 187-213.
- (71) Kumar, S.; Tsai, C.-J.; Nussinov, R. *Biochemistry* **2002**, *41*, 5359-5374.
- (72) Kumar, S.; Tsai, C. J.; Nussinov, R. *Biochemistry* **2003**, *42*, 4864-4873.
- (73) Shaw, D. G. *Hydrocarbons with water and seawater*; Pergamon Press: Oxford, 1989; Vol. 37.
- (74) Eliassaf, J. *Journal of Applied Polymer Science* **1978**, *22*, 873-874.
- (75) Chiantore, O.; Guaita, M.; Trossarelli, L. *Makromolekulare Chemie* **1979**, *180*, 969-973.
- (76) Tiktopulo, E. I.; Uversky, V. N.; Lushchik, V. B.; Klenin, S. I.; Bychkova, V. E.; Ptitsyn, O. B. *Macromolecules* **1995**, *28*, 7519-7524.
- (77) Mao, H.; Li, C.; Zhang, Y.; Furyk, S.; Cremer, P. S.; Bergbreiter, D. E. *Macromolecules* **2004**, *37*, 1031-1036.

- (78) Shibayama, M.; Isono, K.; Okabe, S.; Karino, T.; Nagao, M. *Macromolecules* **2004**, *37*, 2909-2918.
- (79) Meersman, F.; Wang, J.; Wu, Y.; Heremans, K. *Macromolecules* **2005**, *38*, 8923-8928.
- (80) Paschek, D.; Nonn, S.; Geiger, A. *Physical Chemistry Chemical Physics* **2005**, *7*, 2780-2786.
- (81) Weissman, J. M.; Sunkara, H. B.; Tse, A. S.; Asher, S. A. *Science* **1996**, *274*, 959-963.
- (82) Schild, H. G. *Progress in Polymer Science* **1992**, *17*, 163-249.
- (83) Maeda, Y.; Higuchi, T.; Ikeda, I. *Langmuir* **2000**, *16*, 7503-7509.
- (84) Maeda, Y.; Nakamura, T.; Ikeda, I. *Macromolecules* **2001**, *34*, 8246-8251.
- (85) Maeda, Y.; Nakamura, T.; Ikeda, I. *Macromolecules* **2001**, *34*, 1391-1399.
- (86) Maeda, Y.; Taniguchi, N.; Ikeda, I. *Macromolecular Rapid Communications* **2001**, *22*, 1390-1393.
- (87) Maeda, Y.; Tsubota, M.; Ikeda, I. *Colloid and Polymer Science* **2003**, *281*, 79-83.
- (88) Maeda, Y.; Yamamoto, H.; Ikeda, I. *Macromolecules* **2003**, *36*, 5055-5057.
- (89) Maeda, Y.; Yamamoto, H.; Ikeda, I. *Colloid and Polymer Science* **2004**, *282*, 1268-1273.
- (90) Lin, S.-Y.; Chen, K.-S.; Run-Chu, L. *Polymer* **1999**, *40*, 2619-2624.
- (91) Katsumoto, Y.; Tanaka, F.; Ozaki, Y. *Kobunshi Kako* **2002**, *51*, 357-366.
- (92) Katsumoto, Y.; Tanaka, T.; Ozaki, Y. *Kobunshi Ronbunshu* **2003**, *60*, 256-268.
- (93) Katsumoto, Y.; Tanaka, T.; Ozaki, Y. *Macromolecular Symposia* **2004**, *205*, 209-223.
- (94) Katsumoto, Y.; Tanaka, T.; Ozaki, Y. *Journal of Physical Chemistry B* **2005**, *109*, 20690-20696.
- (95) Katsumoto, Y.; Tanaka, T.; Sato, H.; Ozaki, Y. *Journal of Physical Chemistry A* **2002**, *106*, 3429-3435.
- (96) Ramon, O.; Kesselman, E.; Berkovici, R.; Cohen, Y.; Paz, Y. *Journal of Polymer Science, Part B: Polymer Physics* **2001**, *39*, 1665-1677.
- (97) Annaka, M.; Amo, Y.; Sasaki, S.; Tominaga, Y.; Motokawa, K.; Nakahira, T. *Physical Review E: Statistical, Nonlinear, and Soft Matter Physics* **2002**, *65*, 031805/031801-031805/031808.
- (98) Annaka, M.; Motokawa, K.; Sasaki, S.; Nakahira, T.; Kawasaki, H.; Maeda, H.; Amo, Y.; Tominaga, Y. *Journal of Chemical Physics* **2000**, *113*, 5980-5985.
- (99) Suzuki, Y.; Suzuki, N.; Takasu, Y.; Nishio, I. *Journal of Chemical Physics* **1997**, *107*, 5890-5897.
- (100) Terada, T.; Inaba, T.; Kitano, H.; Maeda, Y.; Tsukida, N. *Macromolecular Chemistry and Physics* **1994**, *195*, 3261-3270.
- (101) Appel, R.; Xu, W.; Zerda, T. W.; Hu, Z. *Macromolecules* **1998**, *31*, 5071-5074.
- (102) Appel, R.; Zerda, T. W.; Wang, C.; Hu, Z. *Polymer* **2000**, *42*, 1561-1566.
- (103) Tsuboi, Y.; Nishino, M.; Sasaki, T.; Kitamura, N. *Journal of Physical Chemistry B* **2005**, *109*, 7033-7039.
- (104) Wu, Y.; Meersman, F.; Ozaki, Y. *Macromolecules* **2006**, *39*, 1182-1188.
- (105) Zeng, F.; Tong, Z.; Yang, X. *European Polymer Journal* **1997**, *33*, 1553-1556.
- (106) Zhu, P. W.; Napper, D. H. *Journal of Colloid and Interface Science* **1996**, *177*, 343-352.

- (107) Koga, S.; Sasaki, S.; Maeda, H. *AIP Conference Proceedings* **2000**, *519*, 717-719.
- (108) Laszlo, K.; Kosik, K.; Rochas, C.; Geissler, E. *Macromolecules* **2003**, *36*, 7771-7776.
- (109) Miyagishi, S.; Takagi, M.; Kadono, S.; Ohta, A.; Asakawa, T. *Journal of Colloid and Interface Science* **2003**, *261*, 191-196.
- (110) Chauhan, G. S.; Lal, H.; Mahajan, S. *Journal of Applied Polymer Science* **2004**, *91*, 479-488.
- (111) Yu, T. L.; Lu, W. C.; Liu, W. H.; Lin, H. L.; Chiu, C. H. *Polymer* **2004**, *45*, 5579-5589.
- (112) Bykov, S. V.; Lednev, I. K.; Ianoul, A.; Mikhonin, A. V.; Asher, S. A. *Applied Spectroscopy* **2005**, in press.
- (113) Walrafen, G. E. *Journal of Chemical Physics* **1967**, *47*, 114-126.
- (114) Walrafen, G. E.; Fisher, M. R.; Hokmabadi, M. S.; Yang, W. H. *Journal of Chemical Physics* **1986**, *85*, 6970-6982.
- (115) Fujishige, S.; Kubota, K.; Ando, I. *Journal of Physical Chemistry* **1989**, *93*, 3311-3313.
- (116) Reese, C. E.; Mikhonin, A. V.; Kamenjicki, M.; Tikhonov, A.; Asher, S. A. *Journal of the American Chemical Society* **2004**, *126*, 1493-1496.
- (117) Asher, S. A.; Ianoul, A.; Mix, G.; Boyden, M. N.; Karnoup, A.; Diem, M.; Schweitzer-Stenner, R. *J. Am. Chem. Soc.* **2001**, *123*, 11775-11781.
- (118) Mikhonin, A. V.; Bykov, S. V.; Myshakina, N. S.; Asher, S. A. *Journal of Physical Chemistry B* **2006**, *110*, 1928-1943.
- (119) Pimenov, K. V.; Bykov, S. V.; Mikhonin, A. V.; Asher, S. A. *Journal of the American Chemical Society* **2005**, *127*, 2840-2841.
- (120) Song, S.; Asher, S. A. *J. Am. Chem. Soc.* **1989**, *111*, 4295-4305.
- (121) Mikhonin, A. V.; Myshakina, N. S.; Bykov, S. V.; Asher, S. A. *Journal of the American Chemical Society* **2005**, *127*, 7712-7720.
- (122) Song, S. *Analytical Science & Technology* **1993**, *6*, 39-45.
- (123) Harhay, G. P.; Hudson, B. S. *Journal of Physical Chemistry* **1991**, *95*, 3511-3513.
- (124) Takeuchi, H.; Harada, I. *Journal of Raman Spectroscopy* **1990**, *21*, 509-515.
- (125) Walton, A. G.; Rippon, W. B.; Koenig, J. L. *Journal of the American Chemical Society* **1970**, *92*, 7455-7459.
- (126) Chen, X. G.; Asher, S. A.; Schweitzer-Stenner, R.; Mirkin, N. G.; Krimm, S. *Journal of the American Chemical Society* **1995**, *117*, 2884-2895.
- (127) Hudson, B. S. *Proceedings of SPIE-The International Society for Optical Engineering* **1995**, *2524*, 114-124.
- (128) Green, J. H. S. *Transactions of the Faraday Society* **1963**, *59*, 1559-1563.
- (129) Tanaka, C. *Nippon Kagaku Zasshi* **1962**, *83*, 655-657.
- (130) Tanaka, C. *Nippon Kagaku Zasshi* **1962**, *83*, 521-528.
- (131) Tanaka, C. *Nippon Kagaku Zasshi* **1962**, *83*, 661-667.
- (132) Mizutani, Y.; Kamogawa, K.; Kitagawa, T.; Shimizu, A.; Taniguchi, Y.; Nakanishi, K. *Journal of Physical Chemistry* **1991**, *95*, 1790-1794.
- (133) Pimentel, G. C.; McClellan, A. L. *The Hydrogen Bond*, 1960.
- (134) Allerhand, A.; Schleyer, P. v. R. *Journal of the American Chemical Society* **1963**, *85*, 1715-1723.

- (135) Boldeskul, I. E.; Tsymbal, I. F.; Ryltsev, E. V.; Latajka, Z.; Barnes, A. J. *Journal of Molecular Structure* **1997**, *436-437*, 167-171.
- (136) Trudeau, G.; Dumas, J. M.; Dupuis, P.; Guerin, M.; Sandorfy, C. *Topics in Current Chemistry* **1980**, *93*, 91-125.
- (137) Budesinsky, M.; Fiedler, P.; Arnold, Z. *Synthesis* **1989**, 858-860.
- (138) Hobza, P.; Spirko, V.; Selzle, H. L.; Schlag, E. W. *Journal of Physical Chemistry A* **1998**, *102*, 2501-2504.
- (139) Hobza, P.; Havlas, Z. *Chemical Reviews (Washington, D. C.)* **2000**, *100*, 4253-4264.
- (140) Hobza, P.; Havlas, Z. *Theoretical Chemistry Accounts* **2002**, *108*, 325-334.
- (141) Masunov, A.; Dannenberg, J. J.; Contreras, R. H. *Journal of Physical Chemistry A* **2001**, *105*, 4737-4740.
- (142) Hermansson, K. *Journal of Physical Chemistry A* **2002**, *106*, 4695-4702.
- (143) Hermansson, K. *Journal of Chemical Physics* **1993**, *99*, 861-868.
- (144) Hermansson, K. *International Journal of Quantum Chemistry* **1993**, *45*, 747-758.
- (145) Hermansson, K. *Journal of Chemical Physics* **1991**, *95*, 3578-3588.
- (146) Scheiner, S.; Kar, T. *Journal of Physical Chemistry B* **2005**, *109*, 3681-3689.
- (147) Mizuno, K.; Ochi, T.; Shindo, Y. *Journal of Chemical Physics* **1998**, *109*, 9502-9507.
- (148) Wu, S.; Li, H.; Chen, J. P. *Journal of Macromolecular Science, Polymer Reviews* **2004**, *C44*, 113-130.
- (149) Shibayama, M.; Nagai, K. *Macromolecules* **1999**, *32*, 7461-7468.
- (150) Gan, D. J.; Lyon, L. A. *Journal of the American Chemical Society* **2001**, *123*, 7511-7517.
- (151) Donth, E.-J. *Relaxation and Thermodynamics in Polymers. Glass Transition*; Academie Verlag: Berlin, 1992.
- (152) Andrews, E. H. *Fracture in Polymers*; American Elsevier: New York, 1968.
- (153) Sperling, L. H. *Introduction to physical polymer science*; John Wiley & Sons: New York, 1986.
- (154) Matsuoka, S. *Relaxation Phenomena in Polymers*; Hanser Publishers: Munich, 1992.
- (155) Williams, M. L.; Landel, R. F.; Ferry, J. D. *Journal of the American Chemical Society* **1955**, *77*, 3701-3707.
- (156) Mirkin, N. G.; Krimm, S. *Journal of Physical Chemistry A* **2004**, *108*, 10923-10924.